Incorporation of 3-Dimensional ZnO Nanowire Arrays in Bulk Heterojunction Solar Cells

by

Kendall Davis

A thesis

presented to the University of Waterloo

in fulfillment of the

thesis requirement for the degree of

Master of Applied Science

in

Electrical & Computer Engineering

Waterloo, Ontario, Canada, 2020

AUTHOR'S DECLARATION

I hereby declare that I am the sole author of this thesis. This is a true copy of the thesis, including any required final revisions, as accepted by my examiners.

I understand that my thesis may be made electronically available to the public.

Abstract

Organic solar cells have poor charge transport, with carrier mobilities and lifetimes of 3.9×10^{-4} cm^2/Vs and 10^{-4} seconds in P3HT:PCBM devices. This poor mobility leads to higher recombination and lower short circuit current, causing lower power conversion efficiency. It is well known that an optimal nano-morphology for charge transport in organic solar cells resembles highly ordered donor and acceptor domains separated into "pillars" with a separation of twice the exciton diffusion length, allowing any exciton to diffuse to a donor/acceptor boundary horizontally, and allowing the vertical morphology to ensure a direct, phase continuous path for carrier flow to the electrodes. This ideal nano-morphology is very difficult to prepare, with bulk heterojunction devices being able to replicate a diminished version of its advantages.

In this research, a method for incorporating a 3-dimensional front-contact extension composed out of ZnO nanowires in P3HT:PCBM bulk heterojunction solar cells as a way of further replicating the charge collection advantages of the pillared nano-morphology was investigated. This structure should increase electron charge collection by decreasing the distance needed for free charge carriers to travel. The inverted bulk-heterojunction device architecture is chosen because it introduces minimal changes to the standard fabrication process. Nanowires can be easily incorporated into devices by simply adding a hydrothermal growth step after the standard sol-gel ZnO spin coating process. Doing this, it is demonstrated that incorporating ZnO nanowires of carefully controlled height into the conventional bulk heterojunction polymer-fullerene device structure works as a method of increasing short circuit current relative to planar devices with identical fabrication processing. Nanowires of length greater than the active layer thickness are shown to short the device, and so the polymer layer thickness/nanowire length ratio is an important consideration.

Process modification is needed, however, as the presence of ZnO nanowires appears to cause morphological changes that make device destroying PCBM agglomeration a significant issue. By increasing the P3HT:PCBM weight ratio, reducing the trace solvent concentration during the annealing procedure and using a reduced anneal time, this issue can be mitigated. However, the reduction in anneal time also results in lower base level performance for planar devices.

Acknowledgements

I would like to extend sincere gratitude towards Professor William S. Wong for his patience, guidance, and mentorship. I would also like to thank Naeun Kim, Dr. Mohsen Asad, Mohammad Noori, Mozhgan Sadeghianlemraski, Hyunwoo Choi, and Dr. Wontae Park for their advice, assistance and friendship. I would like to thank Richard Barber and Dr. Czang-Ho Lee for their support in the Giga-to-Nanoelectronics (G2N) centre, and Rossi Ivanova for her guidance during my time as a lab teacher's assistant. Finally, I would also like thank my readers, Professors Bo Cui and Lan Wei.

Table of Contents

List of Figures

List of Tables

Chapter 1

Introduction and Background

Due to the many health and environmental negative externalities associated with the use of fossil fuels as the world's dominant energy source, in addition to their finite supply and rising global energy consumption, much investigation into alternative, renewable energy sources has been motivated in recent decades. Out of these alternative energy sources, solar cells, which are solid state electrical devices capable of converting sunlight directly into electricity, have shown remarkable technical and commercial progress in that time.

Industry has decreased the cost of silicon based solar cells from $100 per watt in 1971 to $2.70 per watt for domestic applications and as cheap as $1.13 per watt for large scale utility applications in early 2018 [1]. This allows solar cells to be a competitive renewable energy source. There are many advantages to utilizing solar energy. While not equally effective in all places, solar cells can be used almost anywhere, making them cost effective solutions to energy problems in sunny areas where there is no grid electricity. Solar cells can be easily integrated into existing structures and energy systems. Solar cells produce no noise and release no emissions. They have no moving parts and commercially maintain relatively long lifetimes.

In 2018, 2.2% (1.5% utility + 0.7% small scale) of the total energy produced in the United States was from solar cells [2]. While that number is expected to grow, key disadvantages of solar cells prevent it from not currently being higher. One disadvantage is that solar cells, being reliant on sunlight, can only generate power during the daytime and

under appropriate weather conditions, which makes their output unstable and causes their peak energy production time to be offset from peak energy consumption hours. The primary disadvantage is high cost, with the price of solar panel generated electricity still being higher than the price of electricity generated from most fossil fuel sources in most locations. The crystalline silicon itself, from which a large majority of commercial cells are made, is not cheap. As a result, the price of solar panels are dependent on raw silicon price and processing prices. Other complex issues, such as electricity storage and grid compatibility, need to be addressed for solar energy to be more competitive. Tremendous efforts have been made on these issues, which has helped solar energy adaptation to grow rapidly in recent years. However, to further increase the competitiveness of solar power, massive investments are still needed to further increase cell efficiency and lower panel cost.

Thin film solar cells, devices made by depositing one or more thin layers of photovoltaic material, can reduce solar cell cost by minimizing the use of silicon or substituting it with other materials. They, of course, suffer from low efficiency as well as complex and expensive fabrication processes. Amorphous silicon (a-Si) solar cells are one of three commercially mainstream thin film solar cells. A-Si cells use only approximately 1 % of the silicon needed by typical crystalline-Si cells, making them considerably cheaper, though their efficiency is much lower [3]. Copper indium gallium selenide ($CuIn_{1-x}Ga_xSe_2$ or CIGS) is another mainstream thin film solar cell. CIGS is a direct bandgap semiconductor, and because the material has a high absorption coefficient a much thinner film can be utilized when compared with other semiconductor materials. Cadmium telluride (CdTe) devices are

the predominant thin film technology, accounting for more than half of the thin-film market [4].

Another form of thin film cells are organic solar cells, which are photovoltaic devices that use organic semiconducting materials as an active, energy generating layer. Organic molecules have a high optical absorption coefficient, such that a large amount of light can be absorbed utilizing a small amount of material, usually on the order of hundreds of nanometers in thickness [5]. The materials used in organic solar cells are solution-processable at high throughput and are cheap, resulting in low production costs that can utilize roll-to-roll technologies to fabricate at large volume [5]. Organic molecules are also flexible, making organic solar cells potentially cost-effective for a diverse array of applications. The main disadvantages of organic photovoltaic cells are their low efficiency, strength and stability. Much work is done to improve these areas of performance.

1.1 Operational Principles of Solar Cells

Solar cells operate without an internal power supply and rely on external optical power to generate voltage and current. This energy difference is dissipated as heat. Several key parameters affect the production of high current within the solar cell, such as the active layer material. This layer converts light to free charge carriers which flow to provide current to an external load. It is worth noting that photons with energy smaller than the semiconductor bandgap, a property of materials in the active layer, do not produce electron-hole pairs necessary for current generation inside the device. Conversely, photons with

energies greater than the bandgap do produce electron-hole pairs, regardless of the energy differential [6].

Four different processes should occur to ensure high current density [7]:

1- Absorption of photons from incident light. It is key to take into consideration the light absorption properties of the active layer material, such as the band gap and, for organic cells, the energy level alignment of donor/acceptor molecules [8].

2- Generation of charge carriers (electrons and holes); in the case of organic cells excitons are generated and ideally split into free positive-charge carrier pairs.

3- Charge transport mechanism drives free charge carriers to electrodes with the aid of an internal electric field.

4- Free carriers are collected by properly selected electrodes.

Because solar-cells generate power by producing electrical current for external loads, hindering any of the above processes will decreases the magnitude of the extracted current leading to worse device performance. Large numbers of photons absorbed are not useful if they do not translate into large numbers of free carriers generated, and large numbers of free carriers generated are not useful if they do not translate into large numbers of charges extracted from the device at the contacts. For organic devices, actually extracting carriers is the most significant bottleneck, but each of these factors will be discussed in more detail in later sections.

1.2 Equivalent Circuit

When considering the parameters of a solar cell, it is useful to consider its equivalent circuit. The equivalent circuit diagram of a solar cell is shown in figure 1. It displays the cell current-voltage behavior as being a relationship between four parts: a current source, diode, shunt resistance (R_{sh}) and series resistance (R_s). The current source (I_{ph}) comes from converting absorbed photons to free charge by the solar cell, R_s represents the internal resistance of the cell to current flow, R_{sh} models leakage current through the cell, and the diode represents electron-hole recombination at the p-n junction.

When under open circuit conditions, when the current is zero so I=0, the following circuit equation can be obtained:

$$I = 0 = I_L - I_s \left[\exp\left(\frac{q(V-IR_s)}{nkT}\right) - 1\right]$$

The open circuit voltage (V_{oc}), the difference of electrical potential between two open terminals of the illuminated cell, follows from solving the above equation for V (the voltage across the terminals).

$$V_{oc} = \frac{nkT}{q} \ln\left(1 + \frac{I_L}{I_s}\right) + IR_s$$

Where n the ideality factor, k is the Boltzmann constant, T is temperature, q is the electron charge, and I_L and I_s are the light generated current and reverse saturation current respectively. Flowing charge carriers in the cell are forced to drift to their corresponding electrodes under the internal electric field, where they normally provide power to an external

circuit. Under stable illumination and open-circuit conditions the generated carriers, with no external load to flow to, accumulate on both electrodes, creating a voltage difference. This voltage difference cancels out the built-in potential (V_{bi}). Once canceled, the charge carrier generation and recombination rates are exactly balanced, and no net current occurs inside the device. This leaves the device under quasi-equilibrium condition. The voltage difference between the anode and cathode is the open circuit voltage, the maximum output voltage provided by a solar cell [9]. A direct relation holds between V_{bi}, V_{oc} and the Fermi level (the highest energy that electrons in a material assume at 0 K) E_f, because of this energy level alignment. The result is that V_{oc} can also be expressed as a function of the quasi Fermi level, where E_{Fp} and E_{Fn} are the quasi-Fermi levels under open circuit conditions of holes and electrons respectively, and q is the electron charge.

$$V_{oc} = (E_{Fn} - E_{Fp})/q$$

When under short circuit conditions, in which the two terminals of the cell are connected together with no intermediate external load, $I = I_L = I_{sc}$ (the short circuit current). A plot of the illuminated I-V characteristics of a standard cell can be seen in Figure 1. V_m and J_m are defined as the voltage and current values, respectively, which deliver the maximum power (P_m) as illustrated in Figure 1(b). Due to the impact of the cell active area on the magnitude of photogenerated current, short-circuit current-density (J_{sc}, in units of mA/cm^2) is more commonly used instead of short-circuit current as a way to express the

magnitude of solar cell current. The current density is highly dependent on the power of the incident light source.

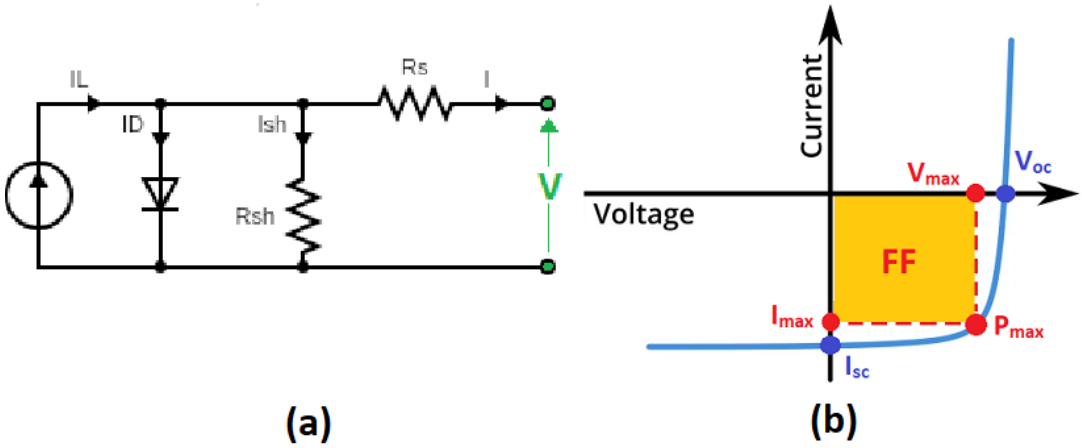

Figure 1 (a) Equivalent Circuit of a solar cell. I_L is the photogenerated current, R_s is the series Resistance, and R_{sh} is the shunt resistance. (b) Current-voltage curve of a solar cell under illumination.

The power conversion efficiency (PCE) of a cell is the ratio of the output electrical power to the input optical power. When the solar cell is operating at maximum power, PCE is expressed as:

$$\mathrm{PCE} = \frac{P_{max}}{P_{in}} \times 100\% = \frac{I_{max} V_{max}}{P_{in}} \times 100\%$$

The fill factor (FF) of a solar cell is the ratio of the solar cell power output (Vmax x Imax) to its ideal power (V_{oc} x I_{sc}). Graphically, FF is the area of the largest rectangle that can be fitted in the J-V curve as seen in Fig.1(b). FF represents the efficiency of charge carrier collection which depends on the charge carrier's mobility, the built-in potential, and

the carrier recombination rate [11]. The largest FF values reported for inorganic solar cells are about 90% while for OSCs values typically range from 50-70% [12-13]. The fill factor is largely determined by R_s and R_{sh}, though there are other factors. Rs has a significant effect on FF, with extremely high values of R_s also leading to a reduction in J_{sc}. In addition to low R_s, a high FF requires large R_{sh} to prevent leakage current.

$$\mathrm{FF} = (\mathrm{I_{max}V_{max}})/(\mathrm{I_{sc}V_{oc}})$$

Series resistance (R_s) and shunt resistance (R_{sh}) are effective parameters which influence the solar cell behavior. The mathematical model for current in the equivalent circuit of a cell with R_s and R_{sh} is [14]:

$$I = I_L - I_s\,[\exp\,(\frac{q(V - IR_s)}{nkT})\,-1]\,-\frac{V - IR_s}{R_{sh}}$$

It has been argued that a dark I-V characteristic is an efficient method to determine Rs using the previous equation for V_{oc} [15]. Because R_{sh} represents cell leakages found under dark conditions when the photocurrent is zero, as R_{sh} approaches infinity the shunt current approaches zero. This is desirable since it is a parasitic current. In optimized solar cells, including organic cells, the shunt current is often negligible [14], therefore R_{sh} is large enough that the last term in the above equation can often be safely ignored. At higher applied voltages when I is much greater than Io :

$$\mathrm{I}\frac{\mathrm{d_V}}{\mathrm{d_I}} = \mathrm{IR_s} + \mathrm{nkT/q}$$

This allows R_s to be extracted from the slope at the high current region of I(dV /dI) vs. I, as shown in Fig.2(A). This can also be done using the slopes of illuminated J-V curves.

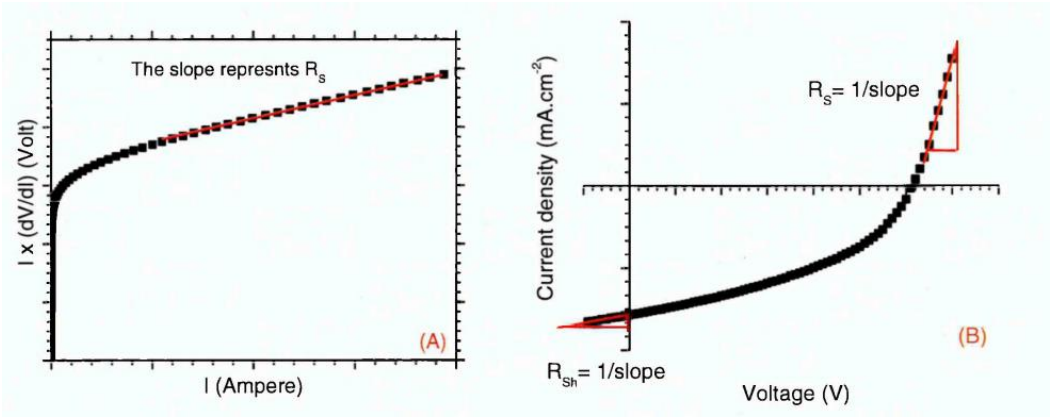

Figure 2 [10] Finding Series and Shunt resistance from (A) Dark J-V and (B) Illuminated J-V

1.3 Organic Solar Cells

Most solar cells are made from inorganic semiconductors such as Si or CdTe. However, organic solar cells are made of polymers and small molecules. These materials are often solution processable, allowing for spin-coating, blade-coating, and printing of thin films (~100 nm) on substrates for device fabrication [16]. These thin films are able to absorb an amount of sunlight that it would take much thicker layers of silicon to absorb due to the typically high absorption coefficient of the organic materials (α = ~6 x 10^5 cm^{-1} for P3HT:PCBM vs ~1 x 10^5 cm^{-1} for CdTe or amorphous silicon for 500nm light). Thus it is possible for organic solar cells to be fabricated with very low costs due to the minimal material use required.

1.3.1 Properties of Conjugated Polymers

Polymers are macromolecules composed of repeating subunits. Organic conjugated polymers are polymers with a "backbone" chain of alternating single and double bonds between carbon atoms. If an electron in Carbon's doubly occupied 2s orbital is energetically excited it may be promoted to its empty 2p orbital. This process allows Carbon to form two additional bonds more than would be expected from standard valence band theory. This is demonstrated in the orbital state configurations seen in Figure 3. In chemical reactions, the formation of the additional bonds releases more energy than was required for the initial electron excitation, making it the energetically favorable state. This explains both the observed high reactivity of CH_2 as well as the stability of CH_4 [17]. Due to symmetries, the system is able to minimize its energy when these bonds are equivalent to each other, which requires that they are formed from equivalent orbitals on the carbon [18]. A set of equivalent orbitals can be obtained that are linear combinations of the valence-shell s and p wave functions. These combinations of orbitals are called hybrid orbitals. The hybrid orbitals sp^3 and sp^2 are of foundational importance in organic electronics.

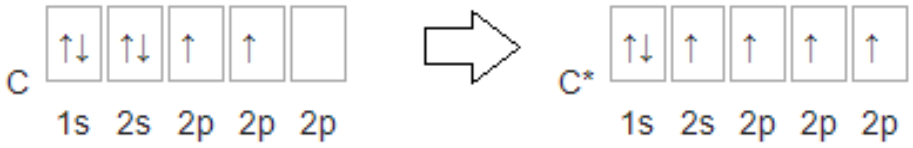

Figure 3 [21] If an electron in Carbon's doubly occupied 2s orbital is energetically excited it may be promoted to its empty 2p orbital

In organic conjugated polymers, the repeating single and double bonds between Carbon atoms and extending along the chain are called “sigma” (σ) and “pi” (π) bonds, respectively [19]. σ-bonds are localized covalent bonds of directly overlapping orbitals. σ-bonds are the strongest form of covalent bonds, and the σ-bonds constituted from directly overlapping sp^3 or sp^2 orbitals are half of the repeating double bonds in conjugated polymers. In addition to σ-bonds, the Carbon double bonds feature a less localized π-bond. π-bonds are covalent bonds in which both lobes of a p orbital on one atom vertically overlap the two lobes of a p orbital on an adjacent atom. π-bonds may form in triple or double bonds but do not typically form in single bonds.

If we consider ethylene (C_2H_4) for example, each carbon atom in a molecule forms three hybridized sp2 orbitals, which each in turn become part of σ-bonds; two C-H bonds and one C-C bond. This leaves each carbon atom with an unbounded valence electron. For geometric reasons these electrons are not able to form a second C-C σ-bond, but still must form a second covalent bond between the carbon atoms in order to fill their outer shells. This requires the atoms to alter the structure of their remaining p orbitals to accommodate the second C-C bond, causing the vertically overlapping π bond. The characteristic of π bonds are the source of the semiconducting properties in conjugated polymers. Because of the delocalization of some electron orbitals as a result of π-bonds, conjugated polymers possess electrical conductivity [20].

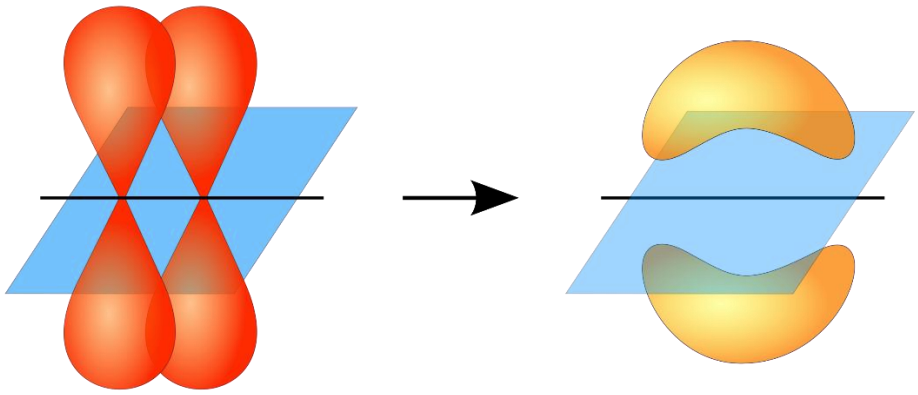

Figure 4 [21] The formation of a π bonds (right) from two p-orbitals (left)

As molecular bonds are formed, electron wave functions between atoms overlap. Due to the Pauli Exclusion Principle, electrons in a molecule are not able to have the same set of quantum numbers. This causes a "splitting", in which the molecular orbital that the overlapping atomic wavefunction would form "splits" into two orbitals, each being a possible configuration for electron clouds to maintain. The higher energy of these potential orbitals is known as the antibonding orbital, due to it being less stable and causing a repulsive bond. In contrast, the lower energy bond is known as the bonding orbital. These are the typical stable bonds that hold molecules together. Because of their lower energy and higher stability, bonding orbitals tend to be filled while antibonding orbitals are typically vacant.

In conjugated polymers the two orbitals created by the overlap of p orbitals in π-bonds are the full π-bonding orbitals and empty π-antibonding (π*) orbitals (the energy band

gap between bounding and antibonding molecular orbitals is larger for the π-π* difference than for the σ-σ* molecular orbitals). The low energy π orbital is also known as the Highest Occupied Molecular Orbital (HOMO), while the higher energy π* orbital is called the Lowest Unoccupied Molecular Orbital (LUMO). The bands formed by these orbitals splitting are analogous to the conduction and valence bands of typical inorganic semiconductors. In an ideal semiconductor, the electronic structure consists of a conduction band and a valence band separated by an energy gap, known as the band gap, the size of which depends upon the energy to break a bond. This gap is analogous to the gap between the HOMO and LUMO level. The difference in energy between the two bands produces the band gap that determines the optical properties of the material. Most semiconducting polymers can be used in optoelectronic devices that work in the optical light range since their band gap lies between 1.5-3.0 eV [22]. Electronic properties of polymers, then, can be described in terms of inorganic semiconductor physics.

Charge transport in conjugated polymers depends on their charge-carrier mobility. Higher charge mobility corresponds to easier charge transportation. The charge-carrier mobility of conjugated polymers is a function of intrachain charge diffusion and interchain interactions [23]. Intrachain charge diffusion depends on the chemical structure and the molecular weight of a polymer, formation of the polymer backbone, the number and nature of defect sites while interchain interactions are governed by the degree of contact, order and orientation of molecules with respect to one another [24].

1.3.2 Principles of Organic Photonics

Organic solar cells are generally made of a series of stacked thin-films in which the active organic layer is sandwiched between two electrodes with work functions chosen for good charge extraction or injection. It is important that one electrode be semi-transparent so that the light may be able to enter the active layer unobstructed. Indium-tin-oxide (ITO) is the most common choice, but metal thin-films can also be suitable. The anode is generally metal, most commonly aluminum, calcium, or magnesium.

In light-emitting diodes (LEDs), electrons are introduced at the low-work function electrode (cathode) with an equal number of holes added at the high-work function electrode (anode) when the diode is under forward bias (the cathode having a lower applied potential compared to the anode). Upon meeting, electrons and holes recombine, with excited electrons in the conduction band relaxing to enter the valence band. The energy is radiated in the form of photons, producing light. A similar, but reversed, process occurs in organic solar cells, in which incident photons excite electrons from the HOMO to the LUMO level, allowing carrier flow from anode to cathode when light is introduced to the cell. However, in the case of solar cells there is no applied voltage during operation.

Figure 5 show the energy level upon light radiation for organic solar cells. When an electron is excited from the HOMO to the LUMO level, an exciton is formed. An exciton is a bound state of an electron and a hole which are attracted to each other by the electrostatic Coulomb force. It is an electrically neutral quasiparticle that exists in insulators and

semiconductors. Excitons are more likely to form in organic semiconductors with their weak molecular forces and charge hopping between localized states.

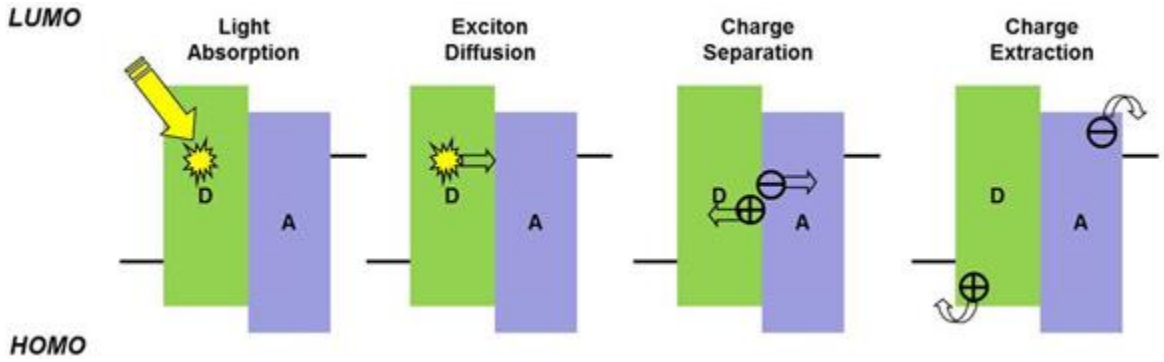

Figure 5 [25] Exciton generation, diffusion, and dissociation

In order for the cell to work effectively it is important that the coulomb force attracting the electron and hole in an exciton be overcome so that the charge carriers may be separated, and the electron and hole can reach opposite electrodes for extraction. The cathode and anode are typically made of different metals, causing the difference in the work function of the electrodes to produce an effective electric field that promotes exciton diffusion to locations with appropriate conditions for exciton dissociation, thereby generating free charges. In summary, a photon is absorbed, creating an excited state electron-hole pair (exciton). The exciton diffuses to a region where charge separation can occur, and then charge carriers are transported to electrodes via an internal electric field generated from electrode work function differences; holes to the anode and electrons to the cathode. This process continues as long as light of an appropriate energy to produce excitons is incident to

the cell, resulting in a current if the electrodes are attached to an external circuit. There are of course loses throughout this process, as excitons may not separate and separated charges may recombine before being extracted if the distance to the electrode is greater than their diffusion length.

In a crystalline inorganic semiconductor with a 3D crystal lattice, the individual energy levels of each atom create a conduction and valence band throughout the material. In most organic semiconductor materials, molecular forces are too weak to create these 3D crystal lattices. Therefore, the molecular LUMOs and HOMOs do not interact strongly enough to create a conduction or valence band. Rather than transport within the band, the charge transport proceeds by hopping between localized states. Utilizing this less efficient movement mechanism means that the carrier mobility of organic and polymeric semiconductors is in general lower than that of inorganic semiconductors. Low dielectric constants in organic semiconductors also creates difficulty for charge separation, leading to a higher propensity for excitons with smaller radii and higher binding energies, called Frenkel excitons.

Exciton dissociation in monolayer organic solar cells occurs primarily at the electrode interface. This means that active layer thickness is an important parameter for device performance. While a thicker layer will obviously lead to increases in photon absorption (and thus increased exciton generation) if the organic layer is too thick then the exciton may be unable to diffuse to an electrode before it recombines and is annihilated. Thus to maximize

current extraction it is important to optimize the device thickness for photon absorption and exciton carrier separation. In most organic solar cells the active layer is on the order of 100nm thick.

1.3.3 Inverted Structure

A drawback of the conventional organic solar cell structure is the difficulty of achieving long-term stability when exposed in air [26]. This is partially due to the use of a low-work-function metals such as aluminum, which is easily oxidized, as a cathode. On the other hand, in the conventional structures, the use of solution-processed contacts such as acidic PEDOT:PSS results in the creation of interfacial layers with typical ITO-coated glass substrates, etching the ITO and degrading device performance.

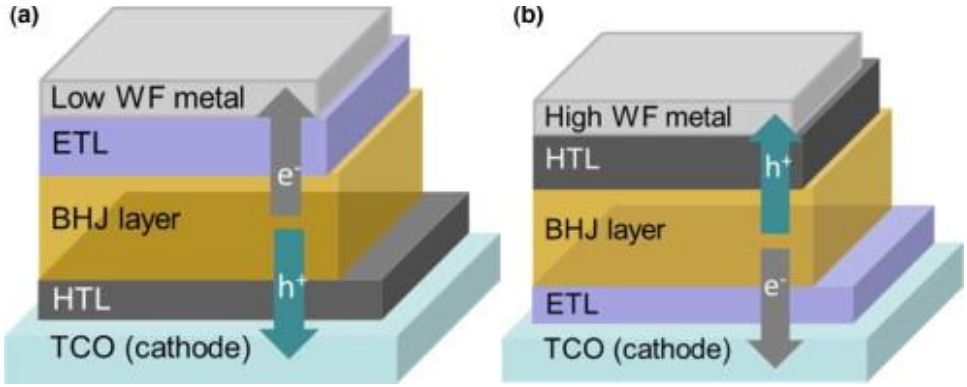

Figure 6 [27] (a) Conventional OPV structure. (b) Inverted structure

Inverted structured devices, in which the charge collection direction is reversed due to reversed electrodes, address these issues. Inverted devices avoid the contact between the PEDOT:PSS and ITO, and the Al for the top electrode typically seen in conventional devices

can be replaced with a more air stable high-work-function metal (like Au or Ag)[28]. Inverted devices show improved ambient stability compared to conventionally structured devices. Additionally, the vertical phase separation in mixed phase polymer-fullerene devices leads to a common polymeric semiconductor, P3HT, being prone to accumulate on the top electrode and the fullerene derivative, such as PCBM, at the bottom, making the reversed electrodes more advantageous for these materials [29].

1.3.4 Bulk Heterojunction Devices

There are several different device configurations for organic solar cells that can be employed. Single layered devices are the simplest. These cells are made by placing a layer of organic semiconductor between two metallic conductors, typically high work function ITO and low work function Aluminum. The work function difference between the two metal conductors creates an electric field in the organic layer. When electrons are excited to the LUMO level by absorbed light, forming excitons, the potential created by the different work functions helps to split the exciton pairs, pulling electrons to the positive electrode and holes to the negative electrode. However, the diffusion length and lifetime (generally on the order of 1ns) of excitons are quite poor, so only a small percentage of generated excitons will be able to make it close enough to the electrodes to have their charge carriers extracted.

In bilayer devices, also known as heterojunction devices, an acceptor and donor are stacked together with a planar interface. By placing two materials with different ionization potentials and electron affinities in contact with one another, a large potential drop is

generated at the donor and acceptor junction which triggers exciton charge separation [30]. Electrons flow to the material with the larger electron affinity while holes move towards lower ionization potential. Due to the energy alignment no band bending occurs. Just as in the single layer device, heterojunction devices are sandwiched between two electrodes for efficient extraction of charge carriers.

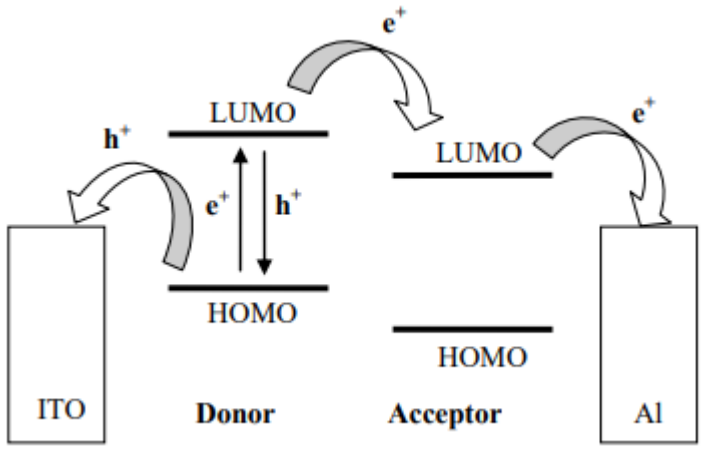

Figure 7 [31] Donor electrons are excited from HOMO to LUMO, leaving a hole. Electrons and holes can recombine, but if there is an acceptor nearby, the electron, preferring the lower energy state, may jump to the acceptor LUMO, separating it from the hole.

In comparison to single-layer devices, recombination in heterojunction devices is significantly decreased and more dependent on trap densities. Electrons travel inside the n-type acceptor and holes travel inside the p-type donor material more effectively after the exciton dissociation at the materials interface. The photocurrent is linearly dependent on the

illumination intensity [32], and a larger fill-factor can be achieved by using a thinner organic layer [33]. Heterojunction device can be fabricated either by using thermal evaporation to consecutively deposit the two materials or by using solution casting of one soluble material layer and evaporation process for the second layer.

However, because exciton dissociation mainly occurs at the donor/acceptor interface, the formation of excitons needs to be within the exciton diffusion length of the interface in order for most carriers to be separated. The diffusion lengths are around 10 nm for most common materials, once again greatly limiting the volume from which charge can be effectively extracted. Planar heterojunction cells must be thin to enable successful diffusion to contacts, but as noted previously, thinner cells have lower absorption. So while a thicker cell may allow for greater light absorption, only a small fraction of generated excitons will reach the interface and dissociate.

To address this, the acceptor and donor can be blended to form a bulk (or dispersed) heterojunction cell. In this configuration, a donor-acceptor interface is within a distance less than the exciton diffusion length of each absorbing site. In this way, the probability of charge carrier separation for each exciton is greatly increased. Similarly, to bilayer heterojunction devices, there is no energy level alignment and interface effect take place. The operational principle behind the bulk heterojunction cell (BHJ) is the same as that behind the bilayer, but in the bulk heterojunction device there is an exponentially large increase of interfacial area between the donor and acceptor where charge separation occurs. The interfacial area is

dispersed throughout the cell, causing a large decrease in recombination losses due to small exciton diffusion lengths.

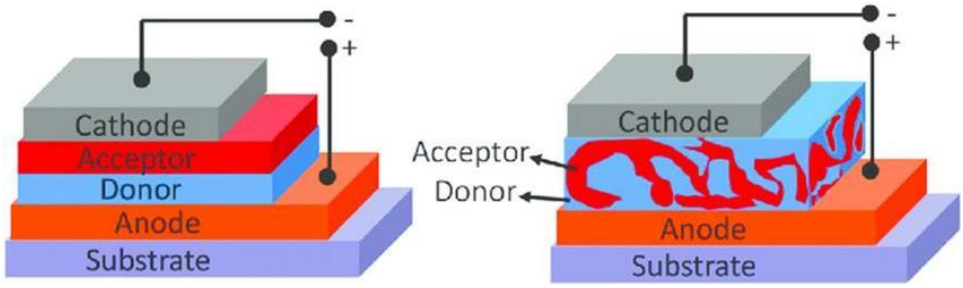

Figure 8 [34] Heterojunction (left) vs Bulk Heterojunction (right) device

Bulk heterojunction devices have greatly increased photocurrent. The nanoscale morphology of these devices is also useful, as the acceptor and donor phases form interpenetrating and bi-continuous networks which act as percolated hole and electron transport pathways to the electrodes.

Bulk heterojunction active layer morphology is greatly impacted by the polymer processing conditions and treatments. Many studies have shown that active layer morphology determines the device performance. There are several ways to control the blend morphology, such as different solvent choices, slow drying of spin-coated films vs. quick drying, altering thermal annealing parameters (anneal time, temperature, annealing in ambient vs vacuum). These fabrication process procedures impact the formation of a phase-separated morphologies between donors and acceptors. For different fabrication processes, experimental procedures need to be optimized to achieve better solar cell performance.

Chapter 2 Bulk Heterojunction ZnO Nanowire Solar Cell

Organic solar cells have poor charge transport, with carrier mobilities and lifetimes of 3.9×10^{-4} cm^2/Vs and 10^{-4} seconds in P3HT:PCBM devices. As discussed, this poor mobility leads to higher recombination and lower J_{sc}, which of course ultimately causes lower PCE. It is well known that an optimal nano-morphology for charge transport in organic solar cells resembles Figure 9, in which highly ordered donor and acceptor domains are separated into "pillars" with a separation of twice the exciton diffusion length. This separation length ensures that any exciton generated in the device is able to diffuse to a donor/acceptor boundary horizontally, and the vertical morphology ensures a direct, phase continuous path for carrier flow to the electrodes. This nano-morphology is very difficult to prepare, with bulk heterojunction devices, which are significantly easier to fabricate, being able to replicate a diminished version of its advantages.

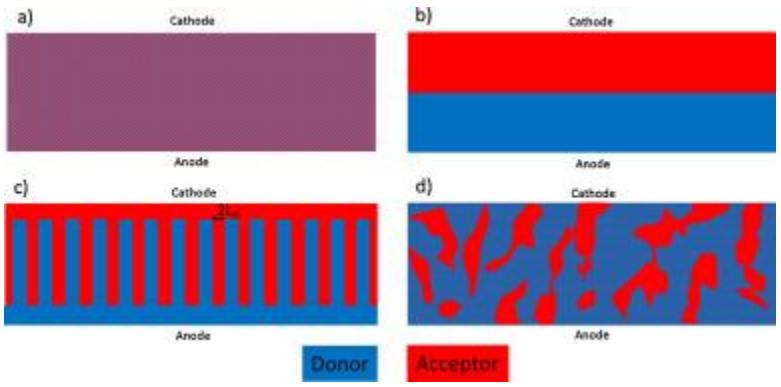

Figure 9 [35] Cross-section schematics of OPV solar cells (a) Very fine mixture of donor and acceptor(b) heterojunction arrangement, (c) ideal morphology of a bulk heterojunction solar cells (d) typical morphology

In this research, a method for incorporating a 3-dimensional front-contact extension composed out of ZnO nanowires, as a way of further replicating the charge collection advantages of the pillared nano-morphology, for use in P3HT:PCBM bulk heterojunction solar cells was investigated.

2.1 Zinc Oxide as an Electron Transmission Layer

Electron transportation layers (ETLs) in polymer solar cells are multi-purpose. They form an effective interlayer for extracting and transporting electrons, they prevent holes from donors entering the cathode, they modify the energetic barrier between active layer and the cathode, and they prevent reactions between the active layer and the cathode. Due to these many functions, it is important for charge collection optimization to select an appropriate material to form an effective ETL. Critical requirements for ETLs in inverted cells include being good at electron extraction and transport, having an energy level suitable to facilitating electron transport, and having high transparency so as to minimize incident optical losses, and high stability.

Semiconducting metal oxides have been investigated for use as ETLs in organic solar cells, with zinc oxide (ZnO), zinc tin oxide (ZTO), titanium sub-oxide (TiOx), aluminum oxide (Al2O3), and niobium pentoxide (Nb_2O_5) being common examples. Out of these materials, ZnO is the most extensively studied for ETLs in inverted polymer solar cells because of its low cost, transparency, environmental stability, suitable energy levels, and high electron mobility [36-37]. ZnO has a conduction band energy of around 4.4 eV and a

valence band energy of around 7.8 eV, which makes it well suited for electron collection and hole blocking from polymer active layer materials. ZnO is also good at reducing charge recombination because of its relatively high electron mobility (~1 cm^2 V^{-1} s^{-1}). While being mostly transparent to visible light, ZnO has an optical cutoff around 375 nm, allowing it to block UV light which protects organic materials from UV photodegradation.[38] ZnO ETLs can also be easily processed via solution methods, and are compatible with both low and high (400-500°C) temperature annealing treatments. As a result, solution processed ZnO ETLs are compatible with roll-to-roll fabrication on flexible plastic substrates.

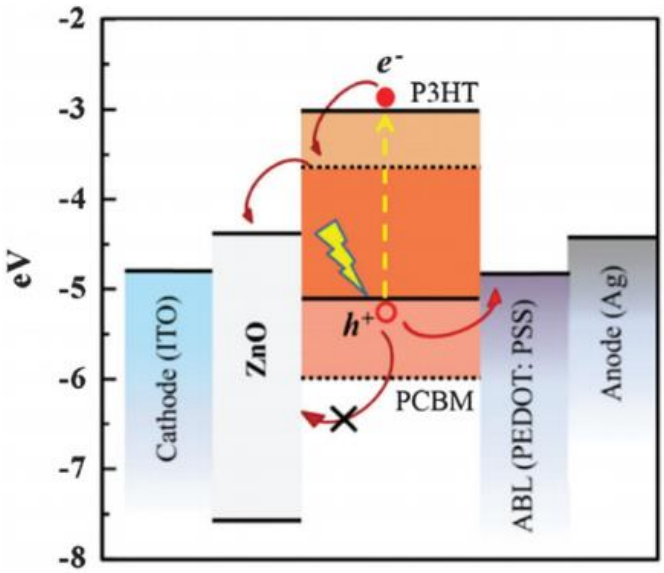

Figure 10 [39] Energy levels and transport directions of carriers in an inverted P3HT:PCBM solar cell with a ZnO cathode buffer layer.

In Figure 10 it can be seen that ZnO's conduction band bottom, at 4.4 eV, is lower than the LUMO of the PCBM, allowing ZnO to effectively extract electrons in the acceptor [41]. Conversely, the valence band of ZnO, at roughly 7.8 eV, is lower than the 5.0 eV HOMO of P3HT, causing an energy barrier which blocks the reverse flow of holes from the donor to the ITO cathode. Because of this ability of ZnO ETLs to prevent generation of leakage current at the polymer/ITO interface, polymer solar cells with ZnO ETLs can improve photovoltaic performance compared to devices without a ZnO ETL [42].

2.2 Zinc Oxide Nanowires

Nanowires are elongated nanostructures with diameters on the order of tens of nanometers. ZnO nanowires (or nanorods) have been widely studied due to their material properties and usefulness in electronics and photonics.

There are many methods for fabricating wurtzite single crystalline ZnO nanorods. The most developed among these is vapor phase growth, in which ZnO vapor condenses onto a solid substrate to form crystalline layers. The ZnO vapor is generated either through chemical reduction (in which zinc vapor from reduced ZnO is transferred to the growth are, followed by reoxidation to ZnO), thermal evaporation (in which commercial ZnO powder is mixed with SnO_2 and evaporated), or from the most common Vapor-Liquid-Solid (VLS) method, in which catalytic droplets are deposited on the substrate and the gas mixtures, including Zn vapor and a mixture of CO/CO_2, react at the catalyst-substrate interface,

followed by nucleation and growth. In all of these processes ZnO nanowires are grown epitaxially on the substrate and assemble into monolayer arrays.

ZnO nanowires can also be grown hydrothermally. The hydrothermally grown nanowires have a hexagonal wurtzite crystalline structure, consisting of a polar surface in the [0001] c-axis direction. Because this surface is energetically favorable to growth, the growth of a 1-D structure is possible [43-44]. The heated aqueous growth solution of zinc nitrate hexahydrate ($Zn(NO_3)_2*6H_2O$) and hexamethylenetetramine (HMTA, C6H12N4) provides the required sources of species for ZnO nanowire synthesis. The chemical reaction for the process is the following:

$$C_6H_{12}N_4 + H_2O \rightarrow 6CH_2O + NH_3 \quad (1)$$

$$NH_3 + H_2O \rightarrow NH_4^+ + OH^- \quad (2)$$

$$Zn^{2+} + 2OH^- \rightarrow Zn(OH)_2 \quad (3)$$

$$Zn(OH)_2 \rightarrow ZnO + H_2O \quad (4)$$

Due to the controlling parameters that exist in the hydrothermal approach to assist growth, the process can be easily tweaked to synthesize the desired nanostructures.

2.3 ZnO Nanowire P3HT:$PC_{60}BM$ Solar Cell

3-Dimensional pillared contacts that can penetrate the active layer should be able to replicate charge transport benefits of the ideal, perfectly phase separated, pillared

donor/acceptor nanomorphology. For exciton separated charge carriers, these contacts can reduce the distance required of them to travel. Ideally, by separating the contacts by twice the length of the carrier diffusion, it could be ensured that carriers are able to reach contacts for extraction from anywhere in the device.

This could also lead to the viability of thicker devices. By decreasing the electron diffusion length necessary for extraction, one of the limiting factors of device thickness is removed. In principle nanowire contacts could make the carrier extraction rate constant throughout the active layer, removing any dependency on proximity to the planar back contact. Because thicker material layers will absorb more light, they will also generate more excitons as free carriers. This excess is inefficient in normal devices but could prove to be greatly beneficial in devices with enhanced extraction.

Additionally, while the small, non-ordered phase separation of donors and acceptors in bulk-heterojunction devices are beneficial to exciton charge separation, that many of the domains have no direct path to move their charge to the desired electrode causes some loses.

ZnO sol-gel layers that are frequently used as an ETL in Organic Solar Cells can be used as a seed layer for the growth of ZnO nanowires. The purpose of this research is to incorporate these ZnO nanowires into a conventional inverted P3HT:$PC_{60}BM$ bulk heterojunction cell, for use as an extension of the front-contact. This structure should increase electron charge collection for the reasons outlined, which is of benefit in P3HT:$PC_{60}BM$ devices which can be electron limited dependent on P3HT to $PC_{60}BM$ weight

ratios [51]. This device architecture is chosen because it introduces minimal changes (and ideally, minimal complications) to the fabrication process. As can be seen in Figure 11, the only change in device structure is the inclusion of the ZnO nanowire array on top of the ZnO planar layer. Fabricating this array only requires the introduction of the hydrothermal growth process, which was chosen due to the low-cost processing requirements, lack of required vacuum technology, and simplicity of large area synthesis. Further, this growth process for crystalline ZnO nanowires [45] has been shown to be compatible with fabrication of thin-film solar cells.

In this proposed structure MoO_3 is to be used as the hole transportation layer (HTL). Similarly to the ZnO ETLs, HTLs are used to increase hole extraction from the active layer. PEDOT:PSS is the most commonly used HTL in organic cells, but for inverted devices it is beneficial for device stability and lifetime to use a metal oxide HTL instead of the moisture sensitive PEDOT:PSS.

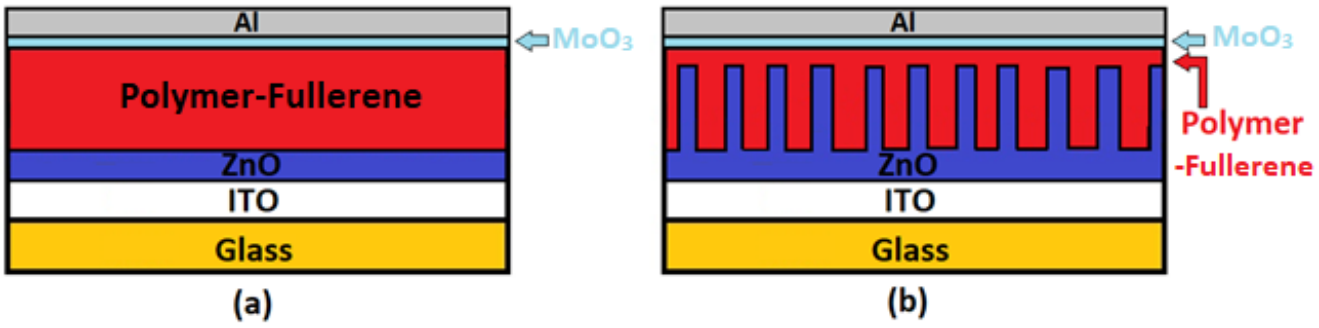

Figure 11 (a) Standard planar version of device (b) proposed nanowire device

Chapter 3 Thin Film Characterization

Thin film solar-cells, of which the nanowire device structure proposed in Chapter 2 is a variant, are composed of a series of layered thin-films. Understanding the key parameters of these material layers and optimizing their quality is critical for understanding and improving device performance. As such, characterizing these layers individually is important. In this chapter the fabrication and characterization of spin-cast ZnO thin films, aqueously grown ZnO nanowires, thermally deposited Aluminum and spin-cast P3HT:$PC_{60}BM$ thin films are detailed.

For the active layer it is important to obtain a structural film of uniform thickness, vertical phase morphological distribution, and high absorption. ZnO thin films should have low absorption while producing well dispersed, sufficiently dense nanowire arrays under aqueous growth conditions that can be controlled to produce nanowires of desired length and diameter. The effects of solution composition, concentration and casting speed on ZnO thin films, as well as nanowire dimensions and density as a function of growth time and casting conditions are reported in this chapter. P3HT:PCBM thin film morphological sensitivity to anneal duration, as well as the resulting agglomeration complications, are also observed.

3.1 Zinc Oxide Thin Films

180mM, 100mM, and 75mM equimolar sol-gel solutions of Zinc Acetate and Ethanolamine in Ethanol were used as a casting solution in spin coating ZnO thin films. Changes in solution concentration lead to changes in film thickness and nanowire density.

For a spin coating speed of 1000 rpm for 30 seconds, each layer had a thickness of roughly 40, 30, and 20nm, respectively. Because the ZnO thin-films are here acting as the ETL in devices with inverted structures, light must pass through the film before it can be potentially absorbed in the active layer. As such, determining the impact of the film thickness on optical absorption is important in determining if a given thickness is a viable option. As can be seen in Figure 12, increasing solution concentrations (corresponding to increasing thicknesses) corresponded to small increases in absorbance, but not enough to block a significant fraction of incoming light above 400 nm, where it is most important for P3HT:PCBM cells.

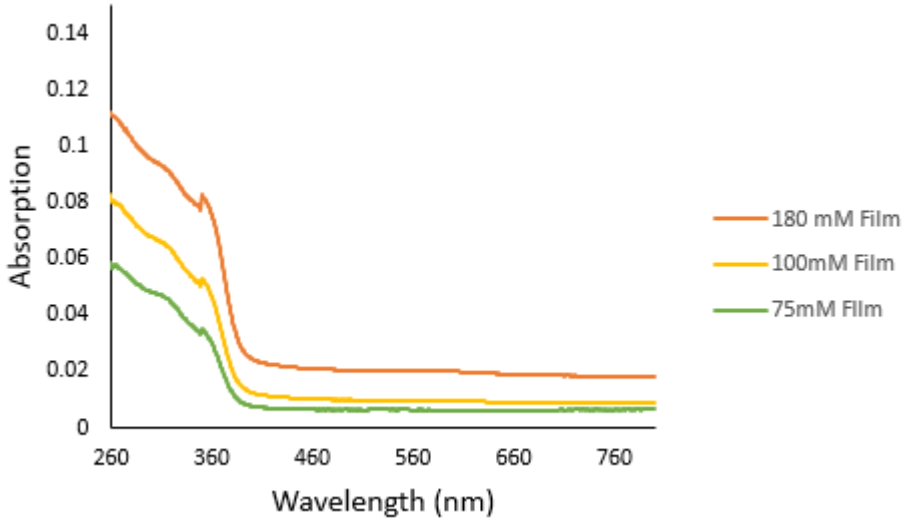

Figure 12 An optical comparison of absorbance for different solutions of ZnO nanoparticles

3.2 Zinc Oxide Nanowire Growth

Initial nanowire array fabrication attempts utilized a well-dispersed aqueous solution of zinc acetate dihydrate ($Zn(CH_3COO)2{\cdot}2H_2O$, Sigma Aldrich) as a casting solution for the

creation of a seed layer for nanowire growth. However, it was found that the films created by this method had extremely poor dispersion, as can be seen in the SEM imagine in Figure 13. Nanowire density varied greatly from region to region, being excessively high in some and excessively low in others. Ideally, a well dispersed film producing nanowires of consistent density corresponding to nanowire pitch roughly the distance of the electron diffusion length (~20nms) would be achieved. To this end, the sol-gel solutions describe in section 3.1 were attempted.

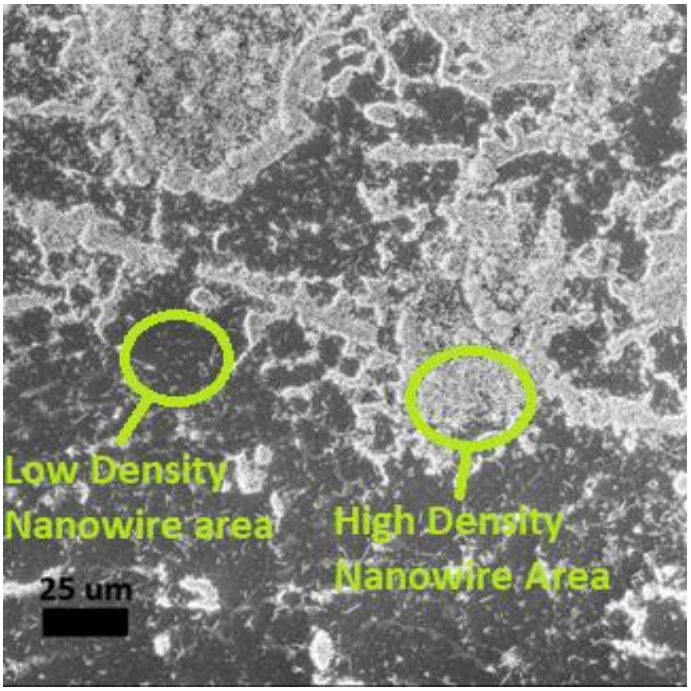

Figure 13 SEM image of a Silicon substrate with ZnO nanowires hydrothermally grown from an aqueous seed layer dispersed by spin coating. Dark regions are the silicon substrate while white areas are regions of high nanowire density, demonstrating very low dispersion.

Zinc Acetate was dissolved in a heated equimolar 100mM solution of Ethanol and Ethanolamine to form a sol-gel casting solution. This sol-gel method provided a uniform film with much better particle dispersion, the results of which can be seen in Figure 14. As mentioned in section 3.1, other solution concentrations were tested as the seed layer but the 100mM solution was selected due to the density of the resulting nanowires, estimated to be 2 $\times 10^{10}$ nanowires per cm^2 via SEM cross-section, which roughly corresponds to a distance between nanowires that is equal to the electron diffusion length in P3HT:PCBM devices.

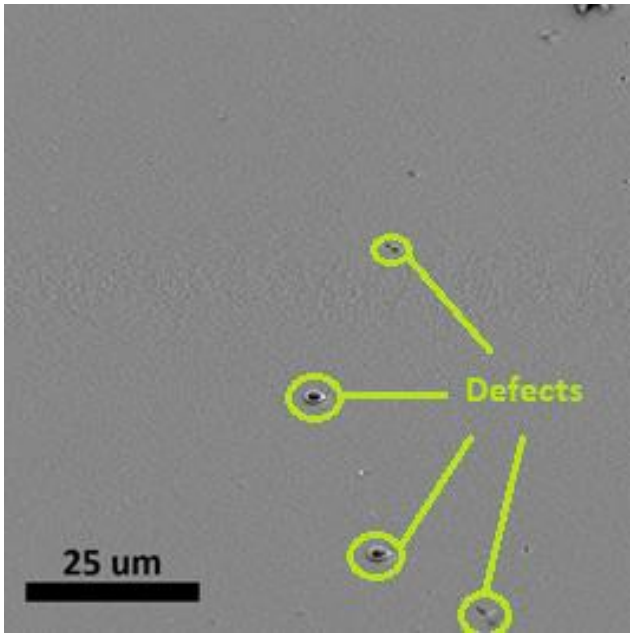

Figure 14 SEM image of a ZnO nanowires hydrothermally grown from a sol-gel seed layer dispersed by spin coating. Good dispersion. Defects can be seen.

Nanowire length was measured via a Zeiss LEO field-emission SEM. The relationship between the nanowire length and growth time was found to be linear, as can be seen in Figure 16.

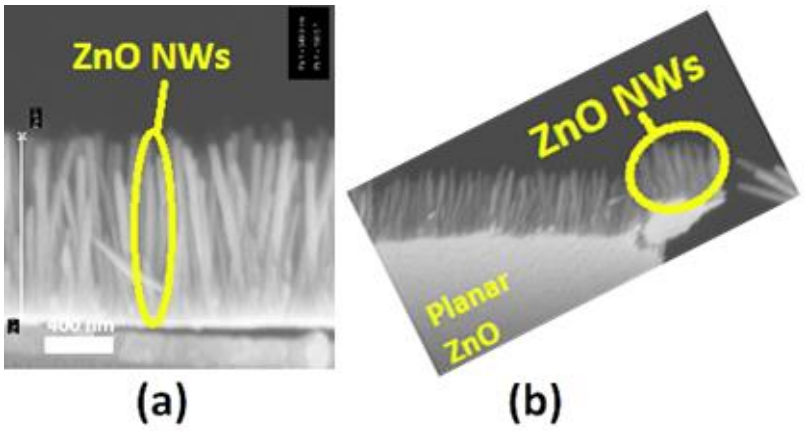

Figure 15 (a) Sideview SEM image of hydrothermally grown ZnO nanowires. (b) Lifted ZnO planar seed layer with nanowires ontop.

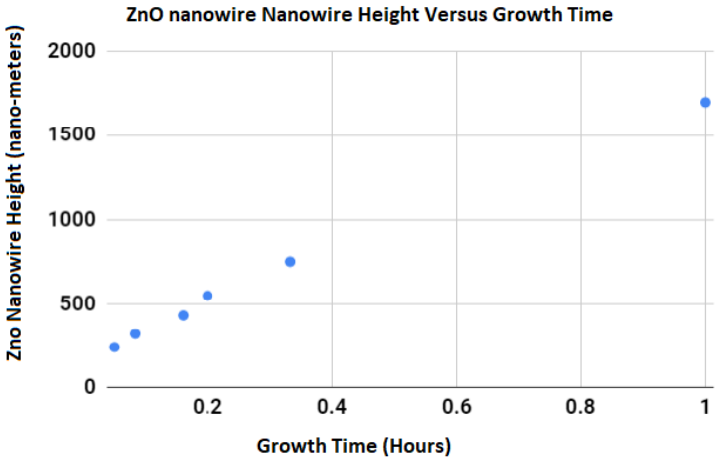

Figure 16 ZnO nanowire height versus growth time

Occasionally, precipitate Zinc Oxide particles from the hydrothermal growth solution will remain on top of the nanowire array despite DI water rinsing. These particles are often an order of magnitude or more larger than the nanowires themselves and can create defects in device fabrication. A more aggressive sonication cleaning step was investigated to alleviate this issue. Nanowire arrays were sonicated at 74khz for 5 minutes in DI water and Isopropanol. A concern was that sonication would lead to damage of the nanowire array. However, SEM images confirm that the arrays were undamaged after sonication.

3.3 Active Layer Characterization

P3HT:$PC_{60}BM$ films were used as a device active layer. This donor/acceptor combination is one of the most common in organic solar cells, with many different weight ratios, solvents, and annealing conditions being investigated for various process optimizations. It is important to be able to produce a structural film of uniform thickness and high absorption.

Initial device thin films were made by spin coating a 45 mg/mL, 1:1 weight ratio solution of P3HT / $PC_{60}BM$ in Dichlorobenzene. These films were spin-cast in a nitrogen environment at various RPM to control thickness and annealed at 170°C for 30 minutes. Film thickness was determined via a Dektak profilometer. Film thickness as a function of spin coating RPM can be seen in Figure 17.

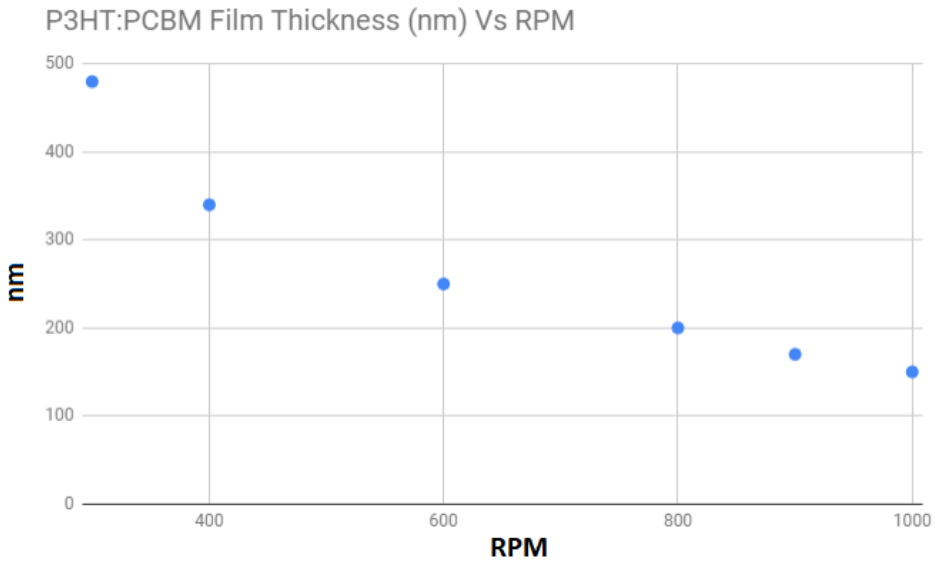

Figure 17 P3HT:$PC_{60}BM$ Thickness vs spin-coating RPM

3.3.2 PCBM Agglomeration

It could be observed optically that for thick films (>200nm) sometimes the morphology of spin coating layers was poor due to agglomeration of PCBM into large particles. This agglomeration did not occur consistently but was always associated with poor performance in planar devices.

It is understood that PCBM agglomeration is greatly aided by trace solvents present in the film and atmosphere [40]. Chang, Jacobs et al. experimentally demonstrated that, as films thermally anneal, solvent evaporates from the bulk heterojunction (BHJ) film only until equilibrium is achieved with the vapor phase, leaving some solvent remaining within the film [40]. Once heat is no longer applied, a new equilibrium is reached in which vapor phase

solvent diffuses back into the film. Their results showed that as long as traces of solvents remain within the layer, PCBM domains continue to quickly grow as the BHJ layer is annealed, and they attribute the morphology and performance variations seen between BHJ devices fabricated in different labs to this phenomenon.

Films were spin-cast on samples in a nitrogen glovebox at various RPM (Figure 17) to control film thickness (more details on this in Chapter 4). As a way of decreasing vapor solvent concentration at the time of anneal, after spin-casting the active layer a 10 minute nitrogen purge was performed in the glovebox. Annealing took place after each purge. It was observed that following this, PCBM agglomeration seemed to decrease in the polymer thin films.

As a way of further decreasing agglomerations, changes to the P3HT:PCBM casting solution were considered. It has been observed in literature that the density and size of PCBM agglomerates in films cast from Dichlorobenzene solvents are greater compared to Chlorobenzene cast films after heat treatment [40], perhaps due to Dichlorobenzene's higher boiling point (bp 180° C) compared to Chlorobenzene (bp 131° C). A spin-casting solution with a higher P3HT:PCBM weight ratio using Chlorobenzene was tried. An optical comparison of the two can be seen in Figure 18. In addition to the resulting spin-cast thin-films indeed appearing to produce fewer agglomerates, optical absorption increased as well, so the Chlorobenzene solution was used moving forward.

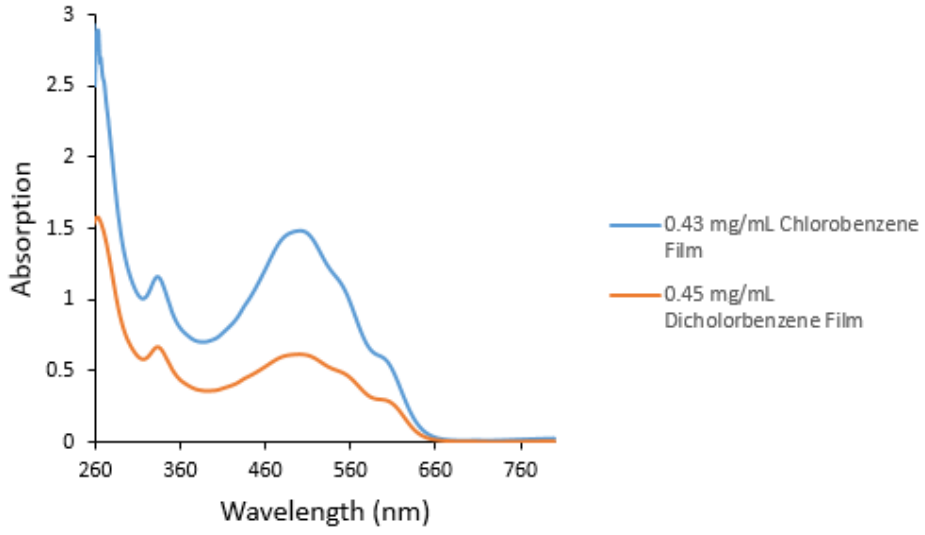

Figure 18 Incident light absorption vs light wavelength for films resulting from different active layer casting solutions

3.3.3 PCBM Agglomeration with ZnO Nanowires

It was further observed that forming the P3HT:PCBM thin-film on top of the zinc oxide nanowire array greatly increased the propensity to form PCBM agglomerates. When annealed under standard conditions of 170° C for 30 minutes in a nitrogen environment, P3HT:$PC_{60}BM$ films on top of nanowire arrays formed large, sometimes 10s of microns in length and several micron in diameter agglomerates. The surface area density of agglomerates varied greatly by region, but in the most impacted areas was on the order of 10^8 per cm^2, as can be seen in Figure 19, and substantially decreased device J_{sc} and V_{oc}.

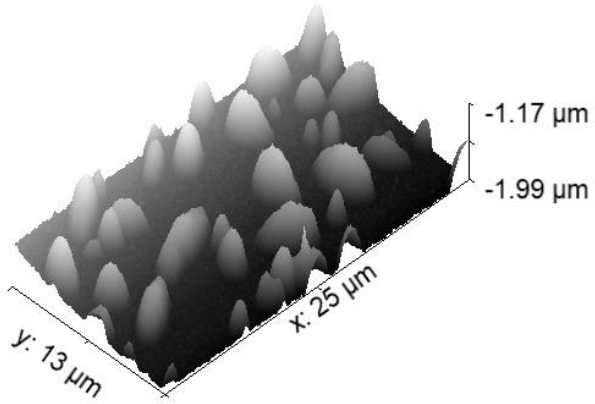

Figure 19 Image from an AFM scan of the surface of the active layer of a device after PCBM agglomerates formed (shown as peaks in the AFM image)

The surface energy change caused by the ZnO nanowire growth likely caused the agglomeration.

In addition to vapor phase solvent concentration, anneal duration and temperature also are factors that can contribute to PCBM agglomeration. Chang, Jacobs, *et al.* observe that prolonged heat treatment at 150°C causes PCBM to diffuse into growing PCBM agglomerates, which acts as a localized sink [40]. This indicates that PCBM has a high mobility within the P3HT matrix at elevated temperatures. The increased diffusion rate leading to the agglomerates is likely the result of a larger amount of solvent remaining within the film or increased surface energy due to nanowires, increasing the diffusion rate of PCBM in the annealing film.

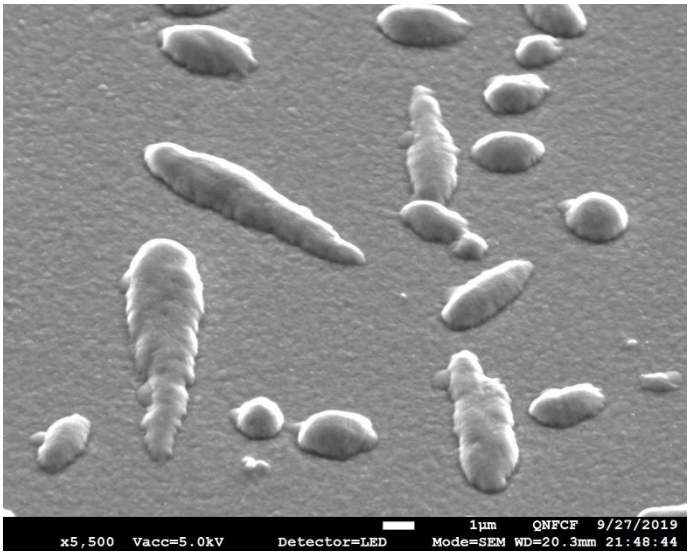

Figure 20 SEM images of the surface of the Al bottom contact after PCBM agglomerates formed

With that information in mind, it was found that reducing the anneal time from 30 minutes to 1 minute would eliminate the agglomeration issue. It was found that reducing the ratio of PCBM to P3HT in the spin-casting solution and changing the solvent from Dicholrobenzene to Chlorobenzene (due to Chlorobenzene's lower evaporation point), both steps that theoretically should make agglomeration less likely [40], did not seem to have notable impact on the agglomeration formation at low anneal times. However, the Chlorobenzene solutions were maintained anyway due to observed higher absorption in spin cast thin films.

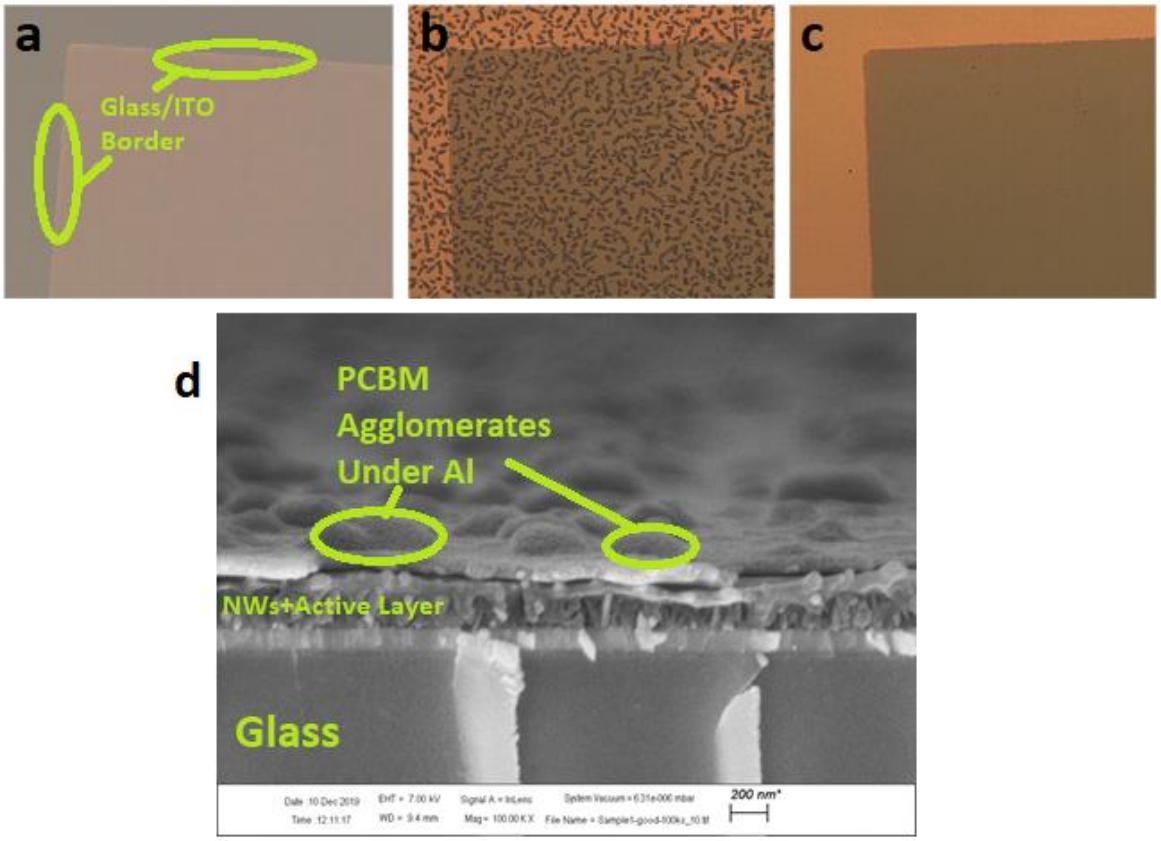

Figure 21 a) Unannealed P3HT:PCBM spin-cast over glass/ITO b) The exact same sample annealed at 170C for 30 minutes c) A different sample annealed for 1 minute d) cross-sectional SEM image of a ZnO Nanowire device with heavy PCBM agglomeration (annealed with same conditions from d).

3.4 Aluminum

Aluminum films were thermally deposited as a bottom contact. The Al film thicknesses were determined via Dektak profilometry of a dummy sample, and ranged from 90 to 110nm. Sheet resistances of 0.1224 ohms per square were typical and determined via 4

point probe measurement. These thickness and sheet resistance values are in line with those commonly used for solar cell contacts [46][47], and at 100nm Al thin films approach their minimum resistivity and maximum reflectance [55].

Chapter 4

Device Fabrication

It is important to use consistent, replicable fabrication steps between experiments to draw conclusions from results. It is also important to develop fabrication procedures that result in functional devices. Descriptions of the device fabrication procedures used for the BHJ organic nanowire solar-cell devices, and motivation behind those choices and steps, are provided in this chapter. Details of substrate cleaning, solution formation, ZnO thin film casting, ZnO nanowire growth, active layer casting, and MoO_3 + Al thermal deposition are given.

4.1 Substrate Cleaning

Prior to nanowire growth, the first step was to ensure clean substrates were used. Glass substrates coated with patterned ITO for use as a transparent front contact were purchased from KINTEC and used for film characterization and device fabrication. Substrates were 1mm thick and 45mm × 45mm in area. They were then further cut into smaller segments of 22.5mm × 22.5mm. All substrates were thoroughly scrubbed and sonicated with Micro 90, followed by a 5-minute DI water sonication. Substrates were then sonicated in Acetone and IPA for 15 and 10 minutes respectively, and subsequently dried using flowing N_2. The substrates were finally subjected to an Inductively-Coupled Plasma Reactive Ion Etch (ICP RIE) oxygen plasma clean to remove any possible remaining residue for 5 minutes using 20sscm of Oxygen, 100mT, and 65 Watts.

4.2 Zinc Oxide Layers

ZnO thin films were prepared via spin coating. 100mM solutions of Zinc Acetate were prepared in Ethanol with 100mM of Ethanolamine. The solutions were heated to 70C and stirred for 1 hour. This results in a solution of suspended ZnO nanoparticles. The solutions were then spin-cast on top of cleaned substrates at 1000 RPM for 30 seconds. Because the ZnO was unpatented it was important to introduce a wiping step to remove the ZnO film from the edges of the substrate as it would otherwise prevent direct contact between the ITO top contacts and the measurement probes, increasing series resistance and decreasing fill factor, as well as possibly causing a short between bottom and top contacts, as seen in figure 22.

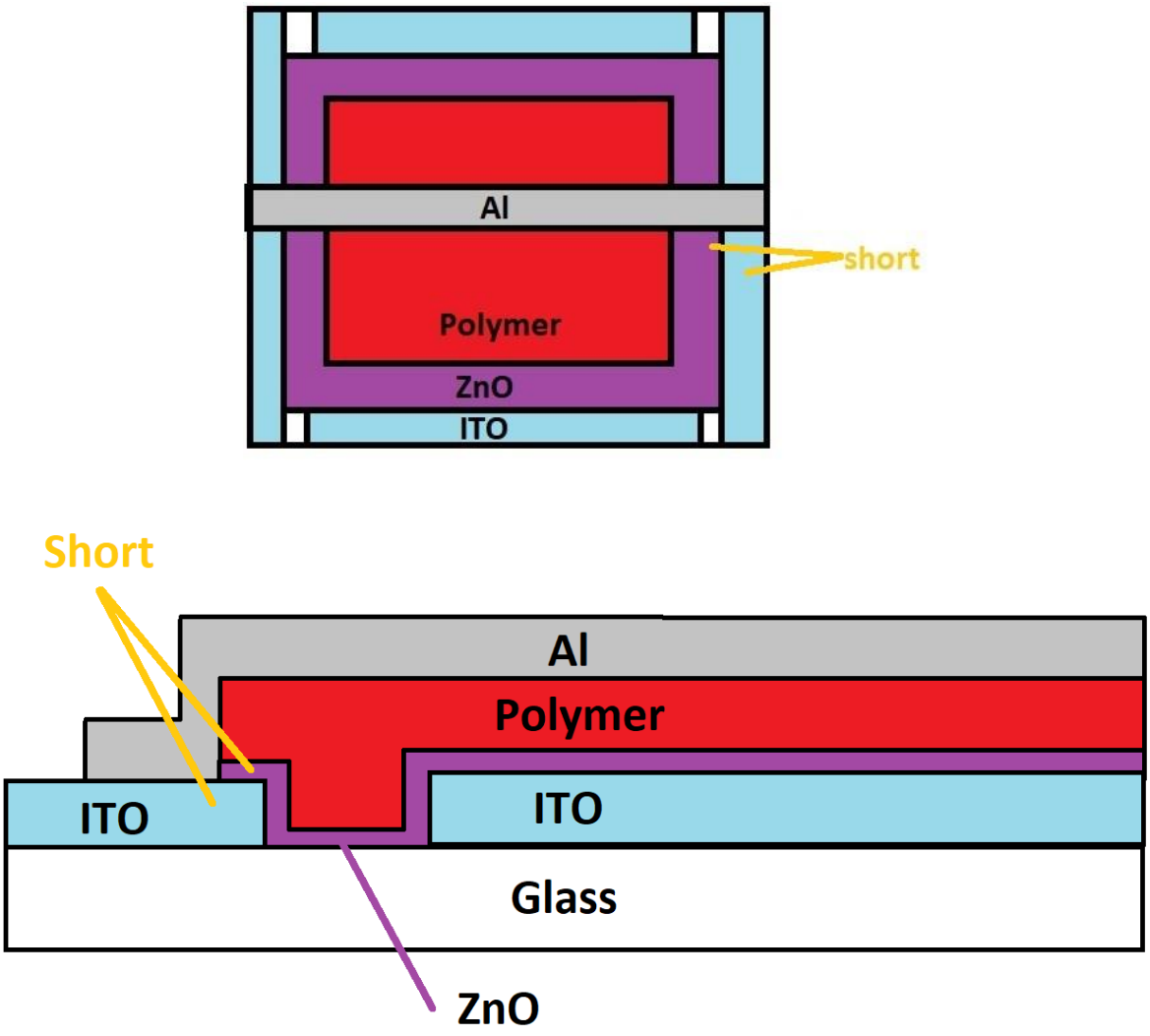

Figure 22 ZnO may potentially short ITO contacts if not removed properly

The wiping was done with cotton swabs dipped in ethanol. After this, substrates were annealed at 350C for 1 hour.

ZnO nanowires were hydrothermally grown in an aqueous 25mM equimolar solution of zinc nitrate hexahydrate (Zn(NO3)2.6H2O, Sigma Aldrich) and hexamethylenetetramine (HMTA, $C_6H_{12}N_4$, Sigma Aldrich). The solution was heated to 90 C in a glass beaker and

stirred via stir bar at 600 RPM. Substrates with ZnO thin films (acting as a seed layer) were suspended from a Teflon holder in solution for between 1 to 30 minutes to control nanowire length and diameter. Substrates were held upside down in solution to prevent precipitate ZnO particles from falling on to the surface. After removal, substrates were rinsed with DI water and sonicated and in DI water and Isopropanol at 74kHz for 5 minutes.

4.3 Active Layer

The active layer of the devices are composed of P3HT:PC_{60}BM polymer-fullerene blends. Two blends were tried: A 1:1 weight ratio of P3HT:PC_{60}BM in Dichlorobenzene and a 1:0.7 of P3HT:PC_{60}BM in Chlorobenzene. Solutions were heated and stirred overnight in a nitrogen environment at 70C. Solutions were then spin coated on top of the ZnO thin films at 600 RPM to produce a thick film. Similar to with the ZnO thin films, in order to expose the ITO front contacts so that the measurement probes could come into direct contact with them, a step in which the polymer film was mechanically wiped away in selected areas was employed. Cotton swabs dipped in small amounts of either Chlorobenzene or Dicholobenzene (corresponding to the solvent of the casting solution) were used to wipe the edges, remove polymer, and expose the desired areas of ITO.

The films would be annealed on top of a hotplate in a nitrogen environment for between 1 to 30 minutes.

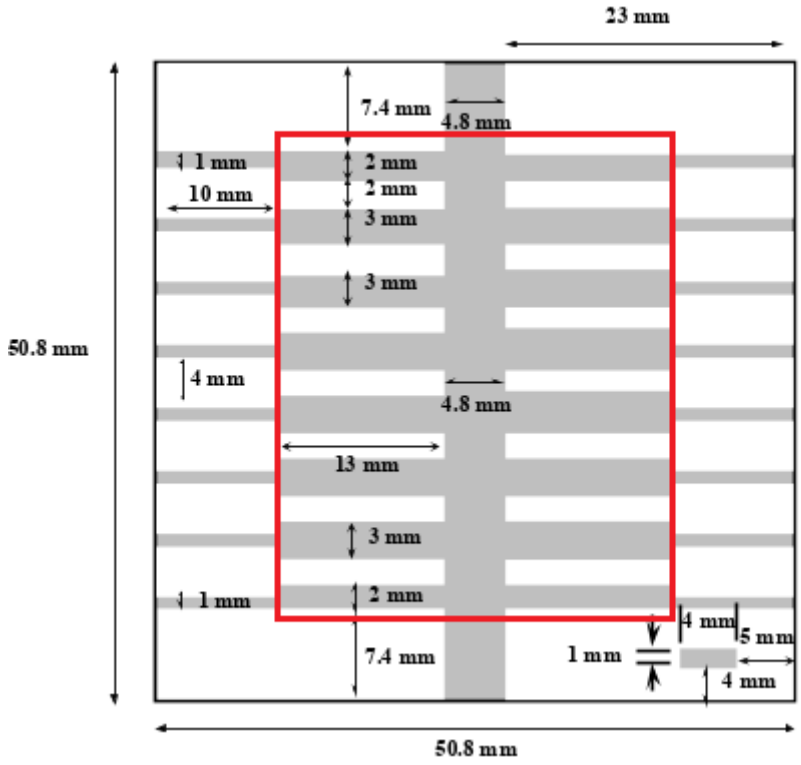

Figure 23 Schematic of the ITO substrates used. White areas are ITO, grey areas are glass. P3HT:PC60BM was spin-cast on top of the entire substrate, but was wiped off of the areas outside of the red square.

4.4 Contacts

Bottom contacts were made of 15-20 ohm/sq ITO on display grade glass, purchased from KINTEC. This sheet resistance is in line with common values for ITO on glass used in organic solar cells, which typically range from 1 to 30 ohm/sq. ITO was chosen due to its transparency (80–95% in the visible range), infrared reflectance >80%, and common use with ZnO thin films as an ETL [50].

A 5 nm layer of MoO_3 was thermally deposited at 0.8 Angstrom per second on top of the polymer active layer to act as a hole transmittance layer (HTL). Much like ELTs, HTLs are used to increase charge extraction of carriers (in the case of HTLs, holes) from the active layer through more favorable material energy level alignment. PEDOT:PSS is the most commonly used HTL in organic cells, but for inverted devices it is beneficial for device stability and lifetime to use a metal oxide HTL instead of the moisture sensitive PEDOT:PSS.

Top contacts of 100nm thick Al thermally were deposited on top of that, initially at 1 Angstrom per second but then ramped up to a fast rate of 10 Angstrom per second. These Aluminum deposition rates were used due to difficulty controlling the evaporation at lower rates with the existing system. At 100nm Al thin films approach their minimum resistivity and maximum reflectance [55].

Fabrication of planar devices was identical to the steps described above but without the hydrothermal growth of ZnO nanowires.

Chapter 5

Device Characterization

By replacing the OSC planar ETL with a hydrothermally grown ZnO nanowire array for use as a 3-dimensional extension of the top contact the transport distance needed for electron extraction at the anode decreases. In this way, due to increased carrier extraction, an improvement in device short-circuit current relative to planar devices was expected for these devices.

This approach introduces a potential issue for increased shunting due to shorts created by the nanowires from the ITO to the aluminum posing cause for concern. Further concerns were that the short anneal procedure adapted in Chapter 4 to prevent PCBM agglomeration may not lead to a high-quality active layer due to a decreased degree of crystallization, and that the quality of active layer phase morphology may be decreased relative to that of planar devices due to different surface energies and coating mechanics on nanowire substrates.

ZnO nanowire OSC device performances are here reported. The impact of nanowire incorporation on short-circuit current and contact effectiveness as a function of nanowire length is first investigated, followed by an investigation on the impact of the annealing procedure by varying anneal temperatures and duration.

5.1 Nanowire Contact Effectiveness

Table 1 shows the device performance for devices with ~300nm thick polymer layers and various nanowire lengths annealed at 170C for 1 minute. Devices with planar ZnO contacts (0 nm in Table 1) were used as reference electrodes. All devices were illuminated under AM 1.5G illumination conditions at 100 mW/cm^2 (ABET Technologies Sun 2000 solar simulator) and measured under nitrogen purge with a Keithley 2400 source meter.

NW Length (nm)	Jsc (mA/cm)	Voc (mV)	FF (%)	PCE (%)
0	5.75 ±1.13	575 ±7.98	37.0 ±0.315	1.23 ±0.312
171 ± 19	6.79 ±1.27	598 ±7.13	33.1 ±1.10	1.34 ±0.284
190± 15	6.45 ±0.912	629 ±24.8	37.6 ±3.64	1.52 ±0.273
221 ± 23	8.16 ±0.325	610 ±3.06	36.7 ±0.605	1.83 ±0.066
252 ± 85	7.66 ±0.897	615 ±4.83	27.9 ±0.315	1.79 ±0.235
285 ± 21	5.81 ±1.15	600 ±4.88	34.6 ±1.92	1.20 ±0.268
405 ± 107	8.34 ±1.36	562 ±34.0	28.7 ±2.06	1.36 ±0.401

Table 1 Parameters of merit for P3HT:PCBM cells annealed at 170C for 1 minute with varying lengths of ZnO Nanowires.

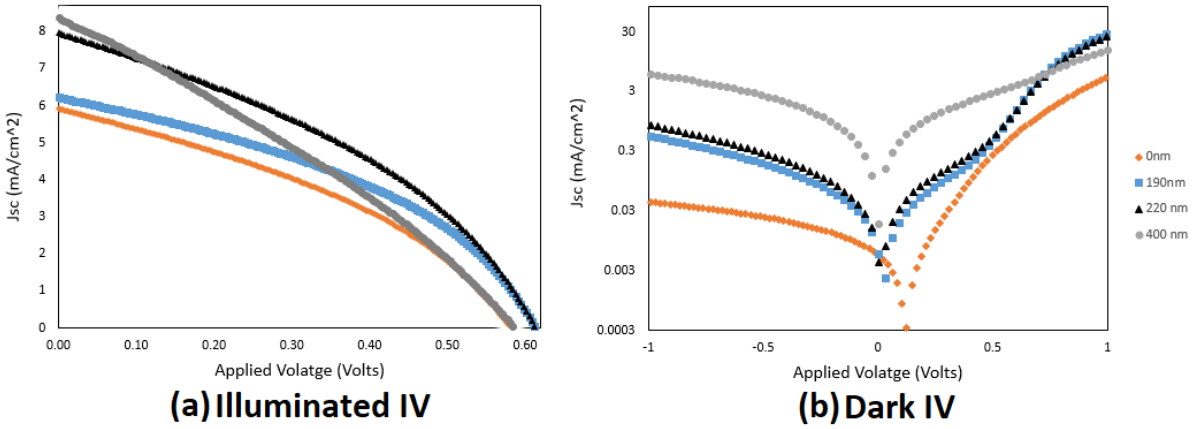

Figure 24 (a) Illuminated IV curves of representative devices annealed at 170C for 1 minute with various ZnO nanowire lengths (indicated by the ledger to the right). (b) Dark IV of the same devices.

Incorporating ZnO nanowires of various lengths into the devices seems to improve device performance on average. For a 300nm thick active layer, ZnO nanowires of roughly are seen to increase device J_{sc}, V_{oc}, and PCE, peaking around 200 nm.

Above 250 nm, device PCE and V_{oc} begin to decrease. This is likely due to an increase in shunting caused by some nanowires piercing through the polymer and directly contacting the MoO_3 or Aluminum. Increasing nanowire length is seen to correspond to higher reverse saturation current, which can be seen in figure 24, and which further points to shunting as an issue. Figure 25 shows average device shunt resistance vs. nanowire length. It is clear that as nanowire length increases shunt resistance tends to decrease. Figure 26 shows nanowire penetration to the top contact as well as a side-view schematic of the penetration.

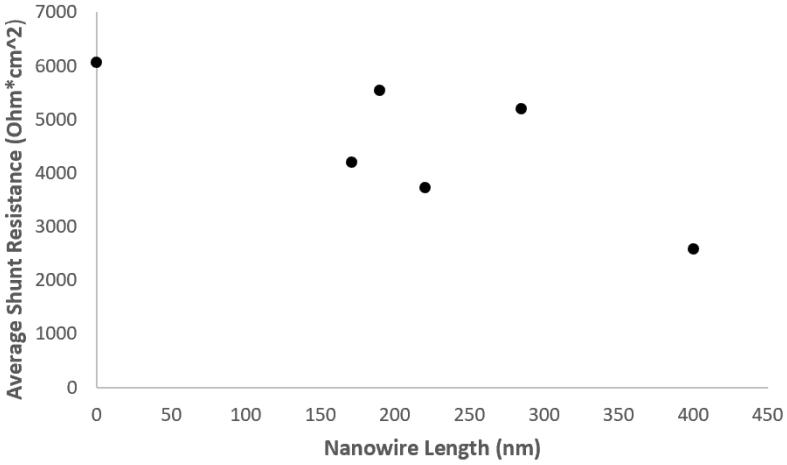

Figure 25 Average Shunt Resistance vs Average Nanowire Length for devices annealed at 170C for 1 minute

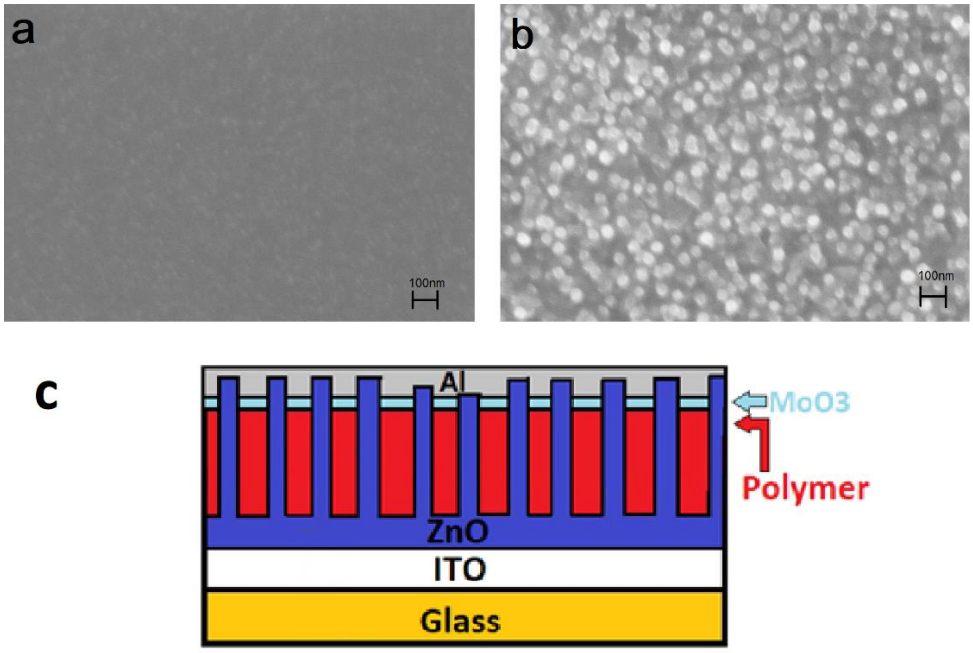

Figure 26 (a) SEM image of top-down view of Al contact on planar device (b) SEM image on top-down view of Al contact of a ~400nm nanowire device, nanowires can be seen (c) Cross section schematic of shorting mechanism

While an increase in J_{sc} was expected, the anticipated impact on V_{oc} for shorter (<250nm) nanometer lengths was less clear. From the Shockley diode equation, we can express the relationship between V_{oc} and J_{sc} in the following way:

$$V_{OC} = \frac{nkT}{q} \ln\left(\frac{J_{SC}}{J_0}\right)$$

This implies that increasing J_{sc} should increase V_{oc}. However, as noted previously, there was concern about the nanowires possibly increasing the reverse saturation current J_o, which would decrease V_{oc}. As can be seen in Figure 24, in all nanowire devices J_o did increase by roughly an order of magnitude relative to reference planar devices, which is a proportionally greater increase than the increase seen in J_{sc} for the same devices. We conclude from this observation that the shunting is dominant.

Physically, an increase in J_o implies that an increase in ideality factor may occur. This is further suggested in the Shockley diode equation by the increase in V_{oc} with nanowire length, despite $\ln(J_{sc}/J_o + 1)$ decreasing. Because in the Shockley diode model it is assumed that ideal photovoltaic devices follow the solar cell current–voltage equation precisely, the diode ideality factor *n* acts as an indicator to describe the difference between the ideal and practical device performance. Typically, the value of the diode ideality factor ranges from 1 to 2 for real devices. $n > 1$ indicates an increase in carrier recombination that may be due to a higher concentration of defect states in the diode. When *n* approaches 2, it suggests that carrier traps become the dominant component of recombination in solar cells. Values greater

than 2 and upwards of 5 are not uncommon in organic solar cells. These values indicate a break in the Shockley model as the devices begin to demonstrate non-diode behavior, often due to shunts or poor active layer/contact interfaces.

Figure 27 shows device ideality factor plotted against nanowire length. An increase in ideality factor with nanowire length is demonstrated. This trend suggests device degradation due to increase in the interface area and the quality of the nanowire sidewall surface, as the surface area of these sidewalls scale linearly with nanowire length. To address these sidewall interface issues, the impact of annealing parameters are investigated in the next section.

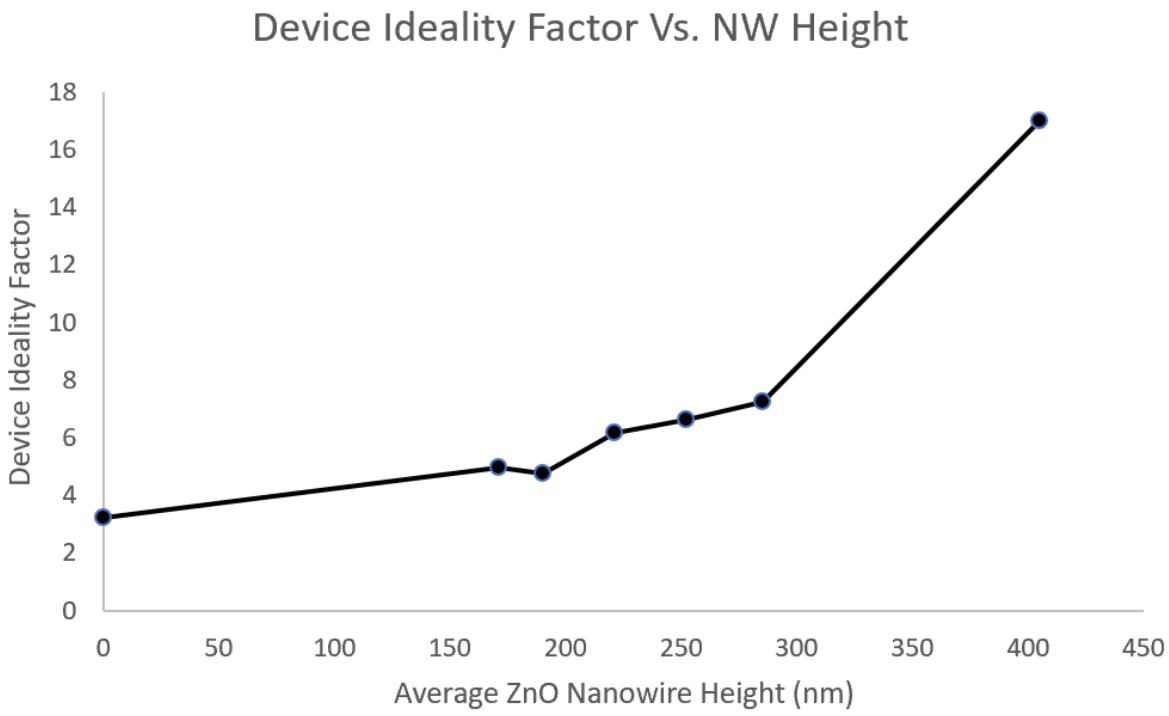

Figure 27 Device Ideality Factor Vs. Nanowire Length

5.2 Impact of Annealing on Surface States

P3HT:PCBM OPV devices are typically annealed to improve phase morphology and P3HT crystallization. Typical P3HT:PCBM OPV anneal times are around 15 to 30 minutes, but as mentioned in Chapter 3, this was found to lead to the formation of large PCBM agglomerates in nanowire devices. Because the anneal time of the devices discussed in section 5.0 (1 min) was significantly shorter than the anneal time of standard planar devices, one might expect the polymer crystallization in these devices to be poor. In addition to increasing carrier mobilities and lifetimes, increased polymer crystallization may decrease polymer/ZnO interface states, and so in an effort to address the rising ideality factor observed in section 5.1, anneal time experiments were performed.

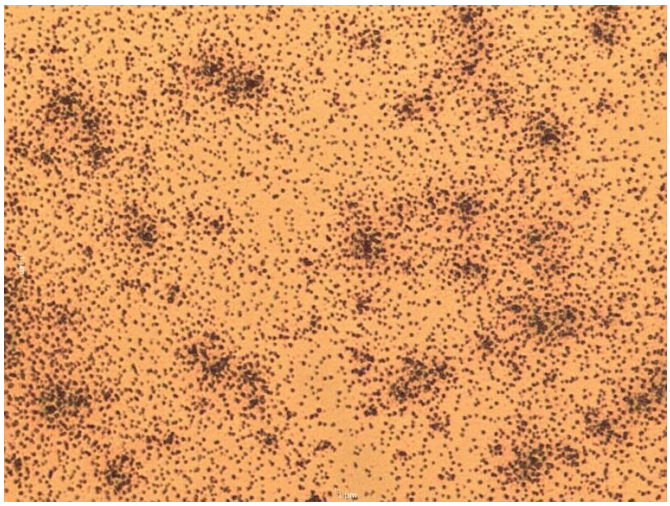

Figure 28 The dark spots are PCBM agglomerates formed from annealing at 170C for 7 minutes

Table 2 shows the parameters of merit for a planar device fabricated under the previously described conditions but annealed at 170C for 30 minutes. Relative to the planar devices annealed for 1 minute, there is a large increase in J_{sc}, FF, and a corresponding increase in PCE. This increase in J_{sc} and FF with anneal duration is a clear result of increased polymer crystallinity and demonstrates that improved anneal conditions alone can yield enhanced device performance relative to the otherwise identical planar devices annealed for 1 minute in section 5.2.

NW Length (nm)	Jsc (mA/cm)	Voc (mV)	FF (%)	PCE (%)
0	8.09	558	54.5	2.47

Table 2 Planar device annealed at 170C for 30 minutes

To optimize anneal time of nanowire devices for improved crystallinity, devices were annealed for between 1 to 7 minutes at 170C. Table 2 shows the results. At a 7 minute anneal time it was found that PCBM agglomerations would form, which can be seen in figure 28. Below that time, V_{oc} appears to increase with anneal duration and average device ideality factors decrease relative to the 1 min anneal devices, as can be seen in figure 29a. These factors imply that prolonged anneals are, as anticipated, somewhat increasing P3HT crystallinity. This is consistent with literature, in which P3HT in polymer-fullerene devices increases its degree of crystallinity significantly and largely stabilizes its grain size over the first 5 minutes of annealing [52][53][54].

Anneal Time (min)	NW Length (nm)	Jsc (mA/cm)	Voc (mV)	FF (%)	PCE (%)
1	220	8.2 ±0.32	610 ±3.06	36.7 ±0.601	1.8 ±0.061
3	180	7.5 ±0.071	620 ±4.07	38.8 ±0.481	1.8 ±0.12
5	200	8.5±0.18	640 ±2.09	40.5 ±1.01	2.2 ±0.073
7	200	3.7±0.21	357±43.3	30.1±1.33	0.40±0.072

Table 3 Parameters of merit for P3HT:PCBM cells annealed at 170C for anneal times of 1, 3, 5 and 7 minutes.

A linear increase in average shunt resistance ($R^2 = 0.9863$) occurred between 1 to 5 minutes, which is shown in Figure 30. This corresponded with a roughly 80% decrease in the average reverse saturation current over the same anneal interval while maintaining the same forward bias current, as can be seen in Figure 29. For the 1, 2, and 3 minute anneal durations the corresponding device ideality factors were 6.3, 4.0, and 2.5 respectively. Based on the degree of P3HT crystallization found over comparable anneal times in literature, as well as observed increased parameters correlated with crystallinity in devices like shunt resistance, fill factor, and V_{oc}, we can surmise that this decrease in ideality factor with anneal duration is likely the result of increased P3HT crystallization, decreasing P3HT/ZnO nanowire interface surface states.

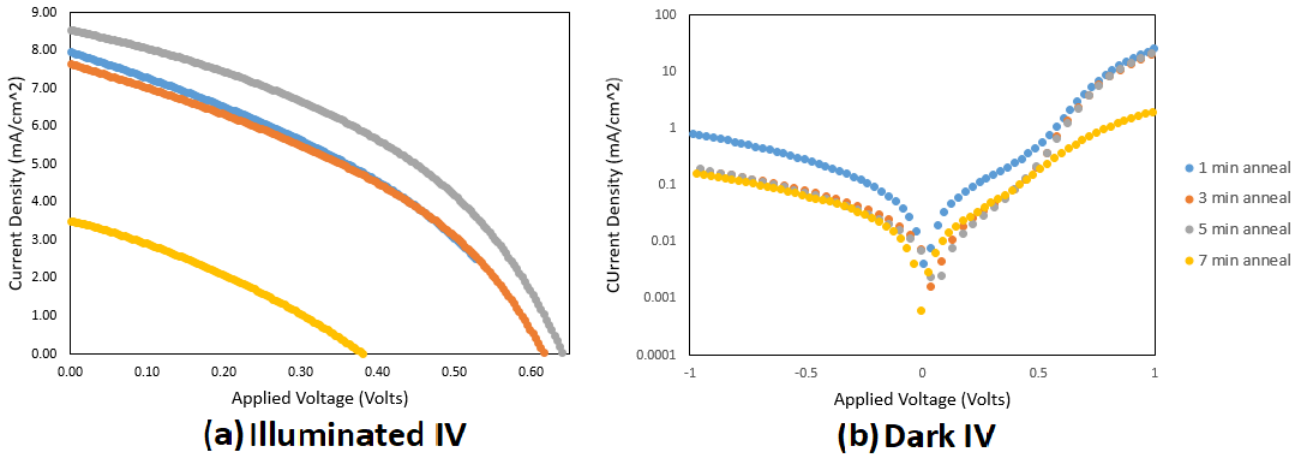

Figure 29 (a) Illuminated IV curves of representative devices annealed at 170C for at various anneal times (indicated by the ledger to the right). (b) Dark IV of the same devices.

After 7 minutes of annealing the lowered reverse saturation current was maintained, however the forward bias current was reduced by an order of magnitude and J_{sc} in illuminated devices decreased by over 50%. This behavior is identical to that observed in other devices in which PCBM agglomeration occurred at large scales. The PCBM agglomeration from these anneal times can be observed in Figure 28. The agglomeration destroys the device morphology, creating pure phase domains that are significantly larger than the exciton diffusion length. It has been shown that film regions with PCBM agglomerates generate very limited photocurrent [40], severely decreasing device performance. At a 7 minutes anneal time the average shunt resistance decreased as a result of PCBM agglomeration, which can be seen in Figure 30.

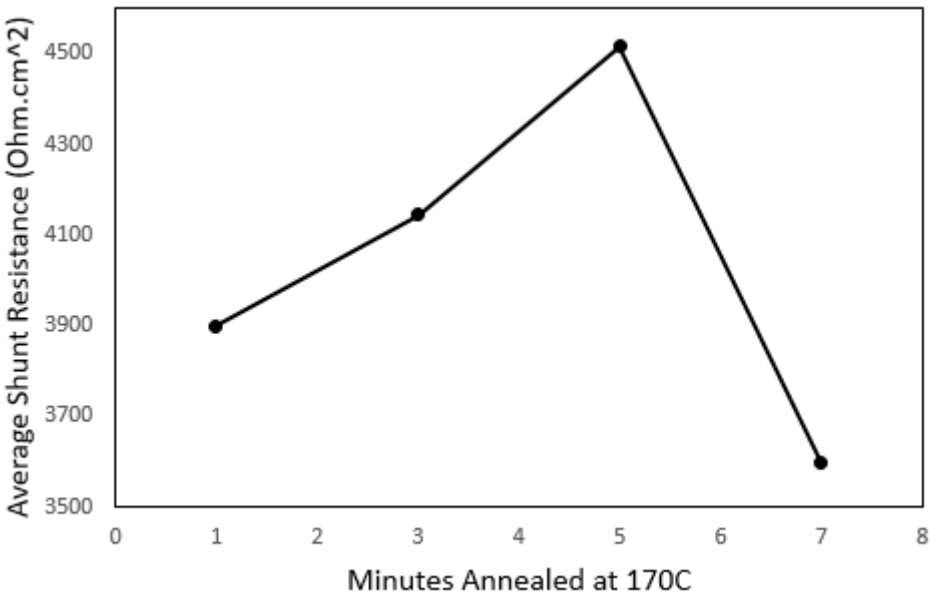

Figure 30 Average Shunt Resistance vs Anneal time for devices annealed at 170C

5.3 Anneal Time Variation at 150C

To observe the effects of anneal temperature in addition to duration, devices were annealed at 150C. Table 3 shows average device performance for these devices annealed for 1 minute.

NW Length (nm)	Jsc (mA/cm)	Voc (mV)	FF (%)	PCE (%)
0	6.80 ±0.801	603 ±9.83	33.5 ±0.450	1.4 ±0.16
150	6.17 ±0.483	572 ±3.93	34.6 ±1.91	1.2 ±0.061
250	9.77 ±0.920	585 ±1.77	29.8 ±0.801	1.7 ±0.12
350	7.17 ±1.41	395 ±99.0	27.7 ±0.693	0.81 ±0.35

Table 4 Parameters of merit for P3HT:PCBM cells annealed at 150C with various nanowire lengths

It is again observed that for devices with ZnO nanowires above 200 nm in length a sizable relative improvement in J_{sc} occurs. Devices with 350 nm nanowires show a sharp decrease in V_{oc} and fill factor, which may be reasonably attributed to shunting due to the nanowires. 150 nm devices are anomalous, showing lower J_{sc} and PCE than the planar devices. This observation suggests a critical nanowire length range may exist under which shunt defects introduced by the nanowires outweigh positive benefits, and above which shunting dominates.

Annealing devices at 150C for 5 minutes produced negligible results. The improvements seen for the devices annealed at 170C for 5 minutes were not observed.

NW Length (nm)	Anneal Time (min)	Jsc (mA/cm)	Voc (mV)	FF (%)	PCE (%)
0	1	6.8 ±0.80	603 ±9.83	34 ±0.45	1.4 ±0.16
	5	6.5± 0.80	580 ±1.82	37± 0.18	1.4± 0.18
220	1	9.8 ±0.92	585 ±1.77	30 ±0.80	1.7 ±0.12
	5	7.9±0.011	550±41.4	35±0.86	1.5±0.11

Table 5 Parameters of merit for P3HT:PCBM cells annealed at 150C for 1 and 5 minutes

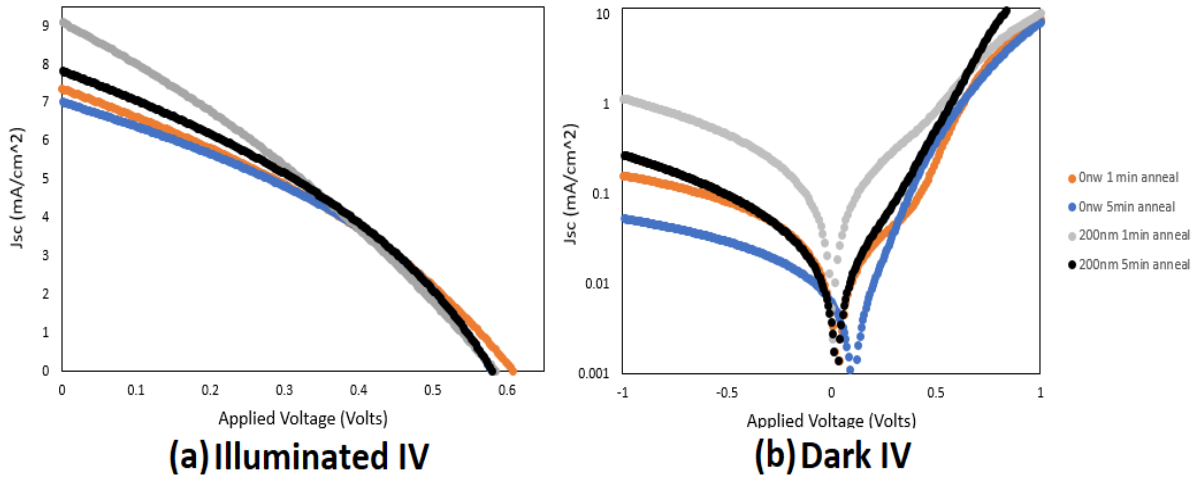

Figure 31 (a) Illuminated IV curves of representative devices annealed at 150C for 1 or 5 minutes (indicated by the ledger to the right). (b) Dark I-V of the same devices.

For devices annealed at 170C a decrease in ideality factor was observed for anneal times up to 5 minutes long, and at 150C another decrease (from 5.1 to 3.3 for planar devices and 6.3 to 4.8 for 220nm nanowire devices) is observed over the same anneal duration. Similarly, the shunt resistance is observed to increase (from ~5700 to ~6100 ohm·cm^2 for planar devices and ~3800 to ~4500 ohm·cm^2 for 220nm nanowire devices) over this range. Decreasing ideality factors with anneal time along with increasing shunt resistances with anneal time suggests an improved degree of crystallinity and a decrease in defects.

By annealing devices at 150C for 5 minutes, a drop in V_{oc} (~600mV to ~580mV and ~585mV to ~550mV for the planar and 220nm nanowire devices, respectively) and J_{sc} (~9.5mA/cm^2 to 7.5mA/cm^2 for the 220nm devices) are observed. It is difficult to explain a drop in both J_{sc} and V_{oc} caused by annealing. A V_{oc} reduction with anneal time is commonly observed in P3HT-fullerene devices [48]. As the film is annealed, crystallinity of P3HT increases and the effective bandgap is reduced by increases in the P3HT HOMO level. Since V_{oc} is directly proportional to the difference between the donor HOMO and acceptor LUMO, V_{oc} is reduced with HOMO increases [48]. However this effect was not observed in the devices annealed at 170C, and the same effect that might drive decreased V_{oc} (increased polymer crystallinity) should increase J_{sc}, while instead a decrease is observed. Further study is needed to explain this set of results.

In summary, increased interface states along ZnO nanowires relative to planar thin films, due to some combination of increased surface area or differing fabrication procedures,

lead to an increase in device ideality factor, resulting in lower J_{sc} and fill factor. One way to reduce the number of these interface states is to crystalize surrounding polymer via thermal annealing. To the degree to which this could be done it worked, decreasing ideality factor and improving device performance. However, the surface energy of hydrothermally grown nanowires accelerates PCBM agglomeration, putting strict limits on how long devices can be annealed while maintaining useful functionality. Despite this, it is demonstrated that ZnO nanowires as a front contact extension can be used to increase short-circuit current in inverted organic solar cells. The risk for shunting (observed as a decreased shunt resistance), poor interface quality (observed in a high ideality factor), and increased defects must be mitigated in addition to the increased sensitivity to anneal parameters (observed via increased propensity towards PCBM agglomeration) relative to planar devices. These are crucial considerations and more work is needed to understand their mechanisms. However, the mechanism of improved current extraction via active layer penetrating 3-dimensional contact extensions in organic solar cells has been demonstrated to be a feasible approach for enhancing the charge collection in organic solar cells.

Chapter 6

Conclusions and Future Work

Incorporating ZnO nanowires of carefully controlled height into the conventional bulk heterojunction polymer-fullerene device structure works as a method of increasing J_{sc} relative to planar devices with identical fabrication processing. Nanowires of length greater than the active layer thickness are shown to short the device, and so the polymer layer thickness/nanowire length ratio is an important consideration. Nanowires can be easily incorporated into devices by simply adding a hydrothermal growth step after the standard sol-gel ZnO spin coating process.

Process modification is needed, however, as the presence of ZnO nanowires appears to cause morphological changes that make device destroying PCBM agglomeration a significant issue. By increasing the P3HT:PCBM weight ratio, reducing the trace solvent concentration during the annealing procedure and using a reduced anneal time, this issue can be mitigated. However, the reduction in anneal time also results in lower base level performance for planar devices. Further, reduction in anneal temperature appeared to affect the relative impact of anneal duration on device performance for reasons that are difficult to discern.

For these reasons the improvement observed in this study in device performance granted by ZnO nanowire incorporation must be qualified. Truncating the anneal time

potentially decreases device performance as much or more than nanowire incorporation improves it, seemingly due to lower polymer crystallization. Further experimentation is needed to optimize fabrication processes such that the full benefits of nanowire back-contact incorporation can be realized without diminishing the active layer quality achieved through conventional device fabrication processes.

6.1 Future Work

For future device optimization it is important to be able to take full advantage of the benefits associated with more standard P3HT:$PC_{60}BM$ annealing procedures. To this end, in addition to careful control of atmospheric solvent concentration and other factors with high morphological impact, surface energy modification of the nanowires through either a gentle oxygen plasma exposure or application of a self-assembled monolayer could be of great benefit in reducing nanowire induced morphological changes. Alternatively, solvent additives, such as alkanedithiols, 1-chloronaphthalene, 1,8-diiodooctane, and nitrobenzene have also been thoroughly investigated as a means of reducing PCBM agglomeration and improving BHJ morphology [40].

Additional experiments are needed to explain observed phenomena. A wider set of anneal times that augments conditions presented should be attempted at 150C and below to help explain the behavior of J_{sc} and V_{oc} for those devices. Device anneal time at this temperature should be increased until PCBM agglomerates are observed while observing trends in device performance parameters. If J_{sc} is seen to increase for a 2 or 3 minute anneal

time and then decrease by 5 minutes, this would suggest that lower anneal temperature might be driving faster agglomeration. If decreases relative to the 1 minute anneal in both J_{sc} and V_{oc} hold across all higher anneal times that would suggest the necessity of a temperature above 150C for the process conditions used.

All ZnO nanowire devices studied used the same active layer deposition method resulting in roughly the same active layer thickness of 300nm. Further experiments determining the impact of the anneal temperature and duration on propensity for PCBM agglomeration for different film thicknesses should be conducted. Additionally, as one of the critical advantages of the nanowire incorporation in principle was the ability to utilize thicker active layers for great absorption, it would also be valuable to increase nanowire length with active layer thickness.

Similarly to active layer thickness, a constant nanowire density was used for all fabricated devices. Varying this parameter by changing the spin-casting RPM for the precursor solution may prove useful in changing the effective surface energy and possibly reducing agglomeration propensity but it should be noted that decreasing density by too much would lead to nanowires being further apart than the electron diffusion length (~20nm), and so there is only a narrow range of values to explore (~9×10^{9} cm^{-1} – ~3×10^{10} cm^{-1}), which minimizes the potential benefits. Lower densities may be worth studying but the expected J_{sc} benefits would be lower.

It would also be useful to fabricate devices with more vertically aligned nanowires. This can be done by using sputtering to produce thin seed layers [49]. Spin-cast sol-gel solutions were used to produce seed layers fabrication procedures recorded in this document due to their ease of use and their already common use in P3HT:PCBM OPVs, but the more vertically aligned wires generated from sputtered ZnO seed layers in addition to those layers potentially achieving similar nanowire density at lower thicknesses could be beneficial properties that should be explored.

Bibliography

1. U.S. Solar Photovoltaic System Cost Benchmark: Q1 2018 Ran Fu, David Feldman, and Robert Margolis National Renewable Energy Laboratory
2. "Electric Power Annual 2018", US Energy Information Administration
3. Hart P.R. (1987) Crystalline vs. Amorphous Silicon — a Comparison of their Respective Properties and their Significance in Photovoltaic Applications. In: Goetzberger A., Palz W., Willeke G. (eds) Seventh E.C. Photovoltaic Solar Energy Conference. Springer, Dordrecht
4. Fraunhofer ISE Photovoltaics Report, July 28, 2014, pages 18,19
5. F. Krebs, J. Fyenbo, and M. Jorgensen, "Product integration of compact roll-to-roll processed polymer solar cell modules: methods and manufacture using flexographic printing, slot-die coating and rotary screen printing," J. Mater. Chem., vol. 20, pp. 8994–9001, 2010.
6. Semiconductor Optoelectronics (Farhan Rana, Cornell University), Chapter 5 Photodetectors and Solar Cells
7. S. J. Fonash, (2010). Solar Cell Device Physics, 2nd Ed. Academic Press is an imprint of Elsevier
8. Understanding Energy-Level Alignment in Donor–Acceptor/Metal Interfaces from Core-Level Shifts, Afaf El-Sayed, Patrizia Borghetti, Elizabeth Goiri, Celia Rogero, et. al, *ACS Nano* **2013** *7* (8), 6914-6920
9. Qi, B., & Wang, J. (2012). Open-circuit voltage in organic solar cells. Journal of Materials Chemistry, 22(46), 24315-24325.
10. KADEM, Burak Yahya. (2017). *P3HT:PCBM-based organic solar cells : Optimisation of active layer nanostructure and interface properties.* Doctoral, Sheffield Hallam University (United Kingdom).
11. Ray, B., & Alam, M. A. (2012, June). Achieving fill factor above 80% in organic solar cells by charged interface. In Photovoltaic Specialists Conference (PVSC), Volume 2, 2012 IEEE 38th (pp. 1-8). IEEE.
12. Peng, Y., Zhang, L., & Andrew, T. L. (2014). High open-circuit voltage, high fill factor single-junction organic solar cells. Applied Physics Letters, 105(8), 083304.
13. Meng, D., Sun, D., Zhong, C., et.al. (2015). High-performance solution-processed non-fullerene organic solar cells based on selenophene-containing perylene bisimide acceptor. Journal of the American Chemical Society, 138(1), 375-380.
14. Servaites, J. D., Ratner, M. A., & Marks, T. J. (2011). Organic solar cells: a new look at traditional models. Energy & Environmental Science, 4(11), 4410-4422.
15. Shen, Y., Li, K., Majumdar, N., Campbell, J. C., & Gupta, M. C. (2011). Bulk and contact resistance in P3HT: PCBM heterojunction solar cells. Solar Energy M aterials and Solar Cells, 95(8), 2314-2317.

16. Hoth, C. N., Schilinsky, P., Choulis, S. A., & Brabec, C. J. (2008). Printing highly efficient organic solar cells. Nano letters, 8(9), 2806-2813.

17. David B Cook, *Quantum Chemistry: A Unified Approach*, p.80

18. McMurray, J. (1995). Chemistry Annotated Instructors Edition (4th ed.) Prentice Hall p.272

19. Kalinowski, J. (1999). Electroluminescence in Organics. Journal of. Physics D: Applied Physics, 32 179-250.

20. Roth, S., & Carroll, D. (2004). One-Dimensional Metals: Conjugated Polymers, Organic Crystals, Carbon Nanotubes (2nd Ed ed.). Weinheim, New York: WileyVCH.

21. de.wikipedia - Bild:MOpi.jpg Credit : (in German) MO Pi-Bindung; selbst erstellt; frei verfügbar Original upload : 18:12, 9. Dez 2004 . . Hati .

22. Wallace, G. G., Dastoor, P. C., & Officer, D. L. (2000). Conjugated Polymers: New materials for photovoltaics. Chemical Innovation, 30, 14-22

23. Horowitz, G. (1998). Organic Field-Effect Transistors. Advanced Materials, 10(5), 365-377.

24. Cao, Y., Andreatta, A., Heeger, A. J., & Smith, P. (1989). Influence of chemical polymerization conditions on the properties of polyaniline. Polymer, 30(12), 2305-2311.

25. https://www.sigmaaldrich.com/materials-science/organic-electronics/opv-tutorial.html

26: W. Wong , H. L. Yip , Y. Luo , K. Y. Wong , W. M. Lau , K. H. Low , H. F. Chow , Z. Q. Gao , W. L. Yeung and C. C. Chang , *Appl. Phys. Lett.*, 2002, **80** , 2788 —2790

27. Tzung-Han Lai, Sai-Wing Tsang, Jesse R. Manders, Song Chen, Franky , Properties of interlayer for organic photovoltaics

28: S. K. Hau , H.-L. Yip , N. S. Baek , J. Zou , K. O'Malley and A. K. Y. Jen , *Appl. Phys. Lett.*, 2008, **92** , 253301

29. L.-M. Chen , Z. Xu , Z. Hong and Y. Yang , *J. Mater. Chem.*, 2010, **20** , 2575 —2598

30. Peumans, P., Yakimov, A., & Forrest, S. R. (2003). Small molecular weight organic thin-film photodetectors and solar cells. Journal of Applied Physics, 93(7), 3693-3723.

31. Yusli, Mohd Nizam. "Studies of P3HT:PCBM thin film formation for polymer solar cells / Mohd Nizam bin Yusli." (2013).

32. Halls, J. J. M., & Friend, R. H. (1997). The photovoltaic effect in a poly(pphenylenevinylene)/perylene heterojunction. Synthetic Metals, 85(1–3), 13071308.

33. Tang, C. W., & Albrecht, A. C. (1975). Photovoltai Effects of Metal-clorophyll-a-metal Sandwich Cells. J. Chem. Phys., 62, 2139.

34. Yilmaz, Efe & Yesilyurt, Muhammet & Oner, Volkan & Omeroglu, Gökhan & Özakin, Ahmet. (2017). Operational Stability and Degradation of Organic Solar Cells. Periodicals of Engineering and Natural Sciences

35. Scharber, Markus & Sariciftci, N.S.. (2013). Efficiency of bulk-heterojunction organic solar cells. Progress in polymer science. 38. 1929-1940. 10.1016/j.progpolymsci.2013.05.001.

36. R. Po , C. Carbonera , A. Bernardi and N. Camaioni , *Energy Environ. Sci.*, 2011, **4** , 285 —310

37. S. K. Hau , H.-L. Yip , N. S. Baek , J. Zou , K. O'Malley and A. K. Y. Jen , *Appl. Phys. Lett.*, 2008, **92** , 253301

38. S. Schumann , R. Da Campo , B. Illy , A. C. Cruickshank , M. A. McLachlan , M. P. Ryan , D. J. Riley , D. W. McComb and T. S. Jones , *J. Mater. Chem.*, 2011, **21** , 2381 —2386

39. Liang, Zhiqiang & Zhang, Qifeng & Jiang, Lin & Cao, Guozhong. (2015). ZnO Cathode Buffer Layers for Inverted Polymer Solar Cells. Energy Environ. Sci.. 8. 10.1039/C5EE02510A.

40. Chang, L., Jacobs, I., Augustine, M., & Moulé, A. (2013). Correlating dilute solvent interactions to morphology and OPV device performance. *Organic Electronics*, 14(10), 2431-2443.

41. A. Manor , E. A. Katz , T. Tromholt and F. C. Krebs , *Sol. Energy Mater. Sol. Cells*, 2012, **98** , 491 — 493

42. J.-P. Liu , K.-L. Choy and X.-H. Hou , *J. Mater. Chem.*, 2011, **21** , 1966 —1969

43. L. E. Greene, M. Law, J. Goldberger, F. Kim, J. C. Johnson, Y. Zhang, R. J. Saykally, and P. Yang, "Low-temperature wafer-scale production of ZnO nanowire arrays.," Angew. Chem. Int. Ed. Engl., vol. 42, no. 26, pp. 3031–4, Jul. 2003.

44. L. Vayssieres, K. Keis, A. Hagfeldt, and S.-E. Lindquist, "Three-Dimensional Array of Highly Oriented Crystalline ZnO Microtubes," Chem. Mater., vol. 13, no. 12, pp. 4395–4398, Dec. 2001.

45. L. E. Greene, B. D. Yuhas, M. Law, D. Zitoun, and P. Yang, "Solution-grown zinc oxide nanowires.," Inorg. Chem., vol. 45, no. 19, pp. 7535–43, Sep. 2006.

46. Kadem, Burak & Hassan, A.K. & Cranton, Wayne. (2016). Efficient P3HT:PCBM bulk heterojunction organic solar cells; effect of post deposition thermal treatment. Journal of Materials Science Materials in Electronics. 27. 10.1007/s10854-016-4661-8.

47. Ewelina Krawczak1, Sławomir Gułkowski, "Electrical properties of aluminum contacts deposited by DC sputtering method for photovoltaic applications" , E3S Web of Conferences 19, 03011 (2017)

48. Vandewal, Koen & Tvingstedt, Kristofer & G. Dinku, Abay & Inganas, Olle & Manca, Jean. (2009). On the origin of the open-circuit voltage of polymer-fullerene solar cells. Nature materials. 8. 904-9. 10.1038/nmat2548.

49. Ji, Liang-Wen & Peng, Shi-Ming & Wu, Jun-Sheng & Shih, Wei-Shun & Wu, Cheng-Zhi & Tang, I-Tseng. (2009). Effect of seed layer on the growth of well-aligned ZnO nanowires. Journal of Physics and Chemistry of Solids. 70. 1359-1362. 10.1016/j.jpcs.2009.07.029.

50. Singh, Charan & Anand, Raghubir & Kumar, Jitendra. (2012). Effect of Sheet Resistance and Morphology of ITO Thin Films on Polymer Solar Cell Characteristics. International Journal of Photoenergy. 2012. 6. 10.1155/2012/879261.

51. Mamatimin Abbas, Nalan Tekin. Balanced charge carrier mobilities in bulk heterojunction organic solar cells. Appl. Phys. Lett. **101**, 073302 (2012)

52. Treat, Neil D.; Brady, Michael A.; Smith, Gordon; Toney, Michael F.; Kramer, Edward J.; Hawker, Craig J.; Chabinyc, Michael L. (2011). "Correction: Interdiffusion of PCBM and P3HT

Reveals Miscibility in a Photovoltaically Active Blend (Adv. Energy Mater. 2/2011)". Advanced Energy Materials. **1** (2): 145.

53. Kozub, Derek R.; Vakhshouri, Kiarash; Orme, Lisa M.; Wang, Cheng; Hexemer, Alexander; Gomez, Enrique D. (2011). "Polymer Crystallization of Partially Miscible Polythiophene/Fullerene Mixtures Controls Morphology". *Macromolecules*. **44** (14): 5722.

54. Jo, Jang; Kim, Seok-Soon; Na, Seok-In; Yu, Byung-Kwan; Kim, Dong-Yu (2009). "Time-Dependent Morphology Evolution by Annealing Processes on Polymer:Fullerene Blend Solar Cells". *Advanced Functional Materials*.

55. Abdennaceur Karoui, Aluminum Ultra Thin Film Grown by Physical Vapor Deposition for Solar Cell Electric Nanocontacts, December 2010, ECS Transactions 41(4):21-28